MEV ION BEAM LITHOGRAPHY OF HIGH ASPECT RATIO STRUCTURES WITH A FOCUSED OR APERTURE-SHAPED BEAM FOR APPLICATIONS IN BIOMEDICAL STUDIES AND MICROFLUIDICS

BY
SERGEY GORELICK

Academic Dissertation
for the Degree of
Doctor of Philosophy

Jyväskylä, Finland
September, 2008

MEV ION BEAM LITHOGRAPHY OF HIGH ASPECT RATIO STRUCTURES WITH A FOCUSED OR APERTURE-SHAPED BEAM FOR APPLICATIONS IN BIOMEDICAL STUDIES AND MICROFLUIDICS

BY
SERGEY GORELICK

Academic Dissertation
for the Degree of
Doctor of Philosophy

To be presented, by permission of the
Faculty of Mathematics and Natural Sciences
of the University of Jyväskylä,
for public examination in Auditorium FYS-1 of the
University of Jyväskylä on September 12, 2008
at 12 o'clock noon

Jyväskylä, Finland
September 2008

Preface

I have been very fortunate with my supervisor, Prof. Harry Whitlow, who provided me with an opportunity to do PhD research in such an interesting field where large scale facilities are combined with microfabrication. Harry is a very dynamic and enthusiastic researcher with a well-developed "gut feeling" and I benefited enormously from his broad knowledge and experience. Harry has a very nice personality and he is simply a pleasure to work with.

Dr. Timo Sajavaara is a serious and dedicated researcher who was my other supervisor. Timo is a perfectionist which is often important for producing good quality results and publications. If Harry was my Guru throughout the course of the study, Timo was like a father or a very big brother. He brought me from an infant state of innocent ignorance to the scientific adolescence by slowly teaching all those things that are normally not taught, e.g. unwritten laws of publishing, academic behaviour and the importance of informal interactions (such as those during Fysiikan Päivät).

Mikko Laitinen kept the equipment and the Pelletron running smoothly and helped to fix problems when they arose and I am grateful to him for this. I would like to thank all those people I worked with during the course of this study, such as researcher Paavo Rahkila, Prof. Sulin Cheng and Nitipon Puttaraksa.

I would also like to thank the former and the current Heads of the Physics Departments, Prof. Matti Leino and Prof. Jukka Maalampi, the Head of the Accelerator Laboratory Prof. Rauno Julin and the whole Department of Physics for the warm and cordial working atmosphere.
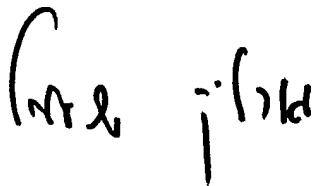
I am thankful to Soili Leskinen, Anna-Liisa Blå, Marjut Hilska and Ritva Väyrynen for their help with the administrative matters.

I spent about six months at the National University of Singapore doing research in the Centre for Ion Beam Analysis (CIBA). The CIBA group was largely brought together by Prof. Frank Watt, who did an excellent job of welding a group with a very informal and family-like atmosphere which makes being in the group a very enjoyable experience. My direct supervisor was Assist. Prof. Jeroen van Kan and I am thankful to him for directing the projects and sharing his knowledge with me. I learned from him a very pedantic and highly critical way of conducting research which I believe is an invaluable skill. The people with whom I shared the office (Isaac Ow, Daniel Parker and Chan Sook Fun), made my stay particularly pleasant. Numerous coffee breaks, lunch breaks and cheerful moments were very nice and I miss them.

Finally, I would like to thank my wife Tiia and daughter Itija for their support and forcing me to come home early, which helped against my workaholic tendencies. I am very grateful to my parents in-law, Miila and Tuomas, whose help and support are acknowledged and appreciated. I wish to thank my parents for their guidance and for unintentionally steering my interest into Physics. My mom has always wanted me to become a gynecologist. I am yet to become a doctor and, even though not a gynecologist (a *real* medical doctor), I know that she feels very proud.

Jyväskylä, September 2008

Abstract

The properties of MeV ions, such as penetration into materials along nearly straight trajectories with minimal scattering and nearly uniform energy loss along the trajectory, make them very useful in microfabrication where tall micro- and nanostructures are required. Such tall structures are important for biomedical research in order to study the response of different cells, e.g. osteoblasts - bone forming cells, to the topography of three dimensional surfaces. Certain surface topographies and the surface chemistry can trigger the osteoblasts grown on such surfaces to start producing bone tissue, which can be utilised for production of artificial bone tissue which can be incorporated into the body.

In a typical MeV ion beam writing tool, the beam of MeV ions, such as protons, from an accelerator is focused into a small beam spot which is then scanned across a photoresist to generate lithographic patterns. This method is very suitable for high resolution work as the proton beams can be focused into small beam spots (tens of nm) using magnetic quadrupole focusing lenses. This method is, however, relatively slow since the patterns are exposed serially, pixel by pixel. In biomedical research, typically large numbers of samples with lithographic structures covering large areas are required.

To overcome the speed limitation of the focused ion beam systems, we developed a novel lithography method, namely Programmable Proximity Aperture Lithography (PPAL). In this method the exposures are performed using a variable-size aperture which shapes the beam spot on the sample and consequently the size of the exposed structure. By combining different sizes of the aperture opening with different positions of the sample relative to the aperture, complex structures made of rectangular elements can be exposed in a short time. The PPAL system is therefore very suitable for fast prototyping of cell growth substrates and microfluidic devices.

Monte Carlo simulation studies using the GEANT4 toolkit were performed to estimate the impact of the ion scattering from the aperture edge on the resolution of the PPAL system. The results indicate that the edge-scattering is not a resolution restricting factor. The contribution to the beam spot broadening from the scattering of ions which are incident on the aperture edge at grazing angles is relatively small but persistent. The simulations indicate, that the primary resolution restricting factor is the beam divergence which results in penumbra broadening of the beam spots.

Experimentally, the smallest line reproducibly written with the PPAL system at the moment in 7.5 μm thick PMMA resist layer is about 300 nm wide on average, which corresponds to an aspect ratio of 25. The aperture edge quality was found to be a second most important resolution restricting factor, as the aperture edge irregularities are reproduced in the pattern edges.

Abstract in Hebrew

ליונים בעלי אנרגיות קינטיות גבוהות (מגה-אלקטרון-וולט, MeV) יש תכונות מיוחדות, כגון יכולת חדירה לתוך חומרים לאורך מסלולים ישירים במינימום של פיזור ואיבוד אנרגיה אחיד (העברת אנרגיה לאטומים ואלקטרונים של החומר). התכונות האלו עושות את היונים המהירים שימושיים מאוד בישומים ליתוגרפיים אם יש צורך ביצירת סטרוקטורות גבוהות עם מידות קטנות (מיקרו- וננו-מטרים). הסטרוקטורות האלו דרושות במחקר ביו-רפואי על מנת לחקור תגובה של תאים שונים, למשל אוסטאובלסטים - בוני עצמות, לתלת-ממדיות של פני השטח אשר התאים גדלים עליהם. טופוגרפיה והרכבה כימית מסוימים של פני השטח יכולים לגרום לאוסטאובלסטים להתחיל ליצור רקמת עצם מלאכותית מחוץ לגוף. את הרקמה המלאכותית יהיה אפשר לכלול לתוך עצם מלאכותי במטרה להשתיל לתוך הגוף.

בתהליך טיפוסי של ליתוגרפיה ביונים בעלי אנרגיה קינטית גבוהה קרן היונים שמגיע ממאיץ חלקיקים ממוקדת לתוך כתם קטן שמסורק על פני הדגם מצופה ב"רזיסט" (חומר פולימרי רגיש לקרינה) באופן דומה מאוד לכתיבה או ציור כדי ליצור סטרוקטורות ליתוגרפיות ברזיסט. השימוש בקרן היונים הממוקדת מאפשר עבודה ברזולוציה גבוהה מכיוון שאת היונים ניתן למקד לכתמים קטנים (עשרות או מאות של ננו-מטרים) בעזרת שדות מגנטיים. לרוע המזל, השיטה הזאת יחסית אטית כי הסטרוקטורות "נכתבות" (נחשפות) באופן טורי - פיקסל אחר פיקסל. זה חסרון של השיטה כי במחקר ביו-רפואי בדרך כלל דרוש מספר רב של דגמים עם הרבה סטרוקטורות שמכסות אזורים גדולים על פני הדגמים.

כדי להתגבר על הגבלת המהירות של החשיפה בקרן היונים הממוקדת פיתחנו באוניברסיטת יובסקולה שיטה ליתוגרפית חדשה. בשיטה החדשה הזאת הדגמים מחושפים דרך מפתח שנמצא בקרבה אל הדגם וששטח הפתח שלו ניתן לשנות. המפתח קובע את הגודל ואת הצורה של כתם היונים על הדגם ובכך את גודל וצורת הסטרוקטורות הנחשפות. על ידי צירוף של צורות הפתח שונות של המפתח עם מיקומים שונים של הדגם ביחס למפתח ניתן ליצור תבניות מרכבות הבנויות מאלמנטים מלבניים בזמן קצר. עקב כך השיטה הזאת מתאימה מאוד ליצירת דגמי-אב לגידול התאים וליצירת דגמים למחקר במיקרופלואידיקה.

כדי להעריך את ההשפעה של פיזור היונים מקצוות המפתח על רזולוציית המערכת ביצענו סימולציות מחשב במסגרת הקוד GEANT4. תוצאות הסימולציות מעידות על כך שפיזור היונים מקצוות המפתח אינו גורם להרחבת כתם היונים על הדגם ואינו מגביל את רזולוציית המערכת. התרומה להרחבת הכתם של היונים שמתנגשים עם פני השטח של קצוות המפתח בזוויות קטנות ומתפזרים מפני השטח יחסית קטנה אבל בלתי זניחה. הגורם העיקרי שמגביל את הרזולוציה הוא התבדרות של קרן היונים שגורמת הרחבה של כתם היונים על הדגם.

הסטרוקטורה הקטנה ביותר שהצלחנו ליצור עד עכשיו בשיטה החדשה היא קיר ברזיסט PMMA שרוחבו 300 ננו-מטרים בממוצע וגובהו 7.5 מיקרו-מטרים (היחס בין הגובה לרוחב הסטרוקטורה 25). התוצאות הניסיוניות מגלות שלאיכות של קצוות המפתח יש חשיבות קריטית ומכריעה על איכות הסטרוקטורות הנוצרות ברזיסטים כי הסטיות של קצוות המפתח מהישרות משוכפלות בקצוות של הסטרוקטורות.

Publications included in the thesis

This thesis is based on the following publications (my contributions are in parentheses).

I. *Growth of osteoblasts on lithographically modified surfaces.* **S. Gorelick**, P. Rahkila, A. Sagari A.R., T. Sajavaara, S. Cheng, L.B. Karlsson, J.A. van Kan, H.J. Whitlow. Nuclear Instruments and Methods B 260 (2007) 130. (Samples surface treatment and preparation, electron beam and UV lithography on SU–8 samples, pattern design for proton beam writing, principal author.)

II. *Adhesion of proton beam written high aspect ratio Hydrogen Silsesquioxane (HSQ) nanostructures on different metallic substrates.* **S. Gorelick**, Z. Fang, J.A. van Kan, H.J. Whitlow, F. Watt. Journal of Vacuum Science and Technology B (2008) submitted. (Sample preparation, sample surface treatment, pattern design, Scanning Electron Microscopy (SEM) characterization of the samples, data analysis, principal author.)

III. *Development of a MeV ion beam lithography system in Jyväskylä.* **S. Gorelick**, T. Ylimäki, T. Sajavaara, M. Laitinen, A. Sagari A.R., H.J. Whitlow. Nuclear Instruments and Methods B 260 (2007) 77. (Took part in designing and assembling the lithography system at the JYFL cyclotron, aligning of the lithography beam line, designed and wrote LabView^{TM} lithography control software, principal author.)

IV. *Programmable proximity aperture lithography with MeV ion beams.* N. Puttaraksa, **S. Gorelick**, T. Sajavaara, M. Laitinen, S. Singkarat, H.J. Whitlow, Journal of Vacuum Science and Technology B (2008) accepted for publication in Sept/Oct. (Led the preparation of the experiments, SEM characterization of the samples, contributed to writing the paper.)

V. *Fabrication of microfluidic devices using MeV ion beam Programmable Proximity Aperture Lithography (PPAL).* **S. Gorelick**, N. Puttaraksa, T. Sajavaara, H.J. Whitlow, Nuclear Instruments and Methods B 266 (2008) 2461. (Led the preparation of the experiments, carried out part of the sample preparation, SEM characterization of the samples, principal author.)

VI. *Aperture edge scattering in MeV ion beam lithography. Part I: scattering from a straight Ta aperture edge.* **S. Gorelick**, T. Sajavaara, H.J. Whitlow. Submitted to Journal of Vacuum Science and Technology B. (Developed simulation code in the GEANT4 framework, performed Monte Carlo studies, analysed the data, principal author).

VII. *Aperture edge scattering in MeV ion beam lithography. Part II: scattering from a rectangular aperture.* **S. Gorelick**, T. Sajavaara, H.J. Whitlow. Submitted to Journal of Vacuum Science and Technology B. (Developed simulation code in

the GEANT4 framework, performed Monte Carlo studies, analysed the data, principal author).

VIII. *Aperture edge scattering in focused MeV ion beam lithography and nuclear microscopy: an application for the GEANT4 toolkit.* **S. Gorelick**, H.J. Whitlow. Submitted to Nuclear Instruments and Methods B. (Developed simulation code in the GEANT4 framework, performed Monte Carlo studies, analysed the data, principal author).

Contents

1 Introduction

1.1 Accelerator-based methods in biomedical studies

In natural tissues the cells are arranged in a three dimensional (3D) organization which provides the appropriate functional, nutritional and spatial conditions. Cellular behaviour in such 3D tissues, e.g. attachment, proliferation, orientation and function, is governed by the surface chemistry of the environment and its topological properties. Artificial cell-growth substrates with modified surface topology can be used to provide detailed information on effects of the surface geometrical properties on the cellular behaviour. This knowledge is important for the success of tissue engineering so that the cells can organize in suitable 3D environment and function properly as tissue. The artificially grown tissue can then be implanted directly into the body, or it can form a part of a device that replaces an organ functionally.

The major reason for this lack of information stems from the general unavailability of precisely patterned 3D substrates where roughness and corners are defined on a nanometre scale. Ion Beam Micromachining is a novel technique that can produce 3D high-aspect ratio micro- and nanomachined surfaces of different shapes and patterns by altering a resist structure, using a beam of high energy ions in a fast and direct write process. The extremely straight and long (10–500 μm) trajectories of MeV ions from accelerators such as the 1.7 MeV Tandem Pelletron or Jyväskylä cyclotron make them a powerful tool for lithographically machining 3D structures on a scale of nm to 100's of μm with walls that are orthogonal to the ion trajectory and with nanometre precision [Watt97]. The most common form of Ion Beam Micromachining, Proton Beam Writing[1] [Watt07], is conceptually similar to the conventional electron beam lithography. A beam of MeV protons from an electrostatic accelerator is magnetically focused into a small beam spot which is then scanned across the resist (in a manner very similar to writing, hence the name "P-beam writing") to generate latent patterns which can later be resolved by development. Because the proton beam can be focused down to very small beam spots (<50 nm [vanK05]) and due to to the ability of MeV ions to penetrate deep into materials along nearly straight paths, 3D nanostructures with extremely high aspect ratios (e.g. ratio between the height of a structure to its width) can be produced (e.g. >150 in SU−8 material [Watt05]). The P-beam writing

---

[1]Here proton beam writing is taken to be exactly what is said. MeV ion beam lithography is more general and also involves the possibility of writing patterns of ion track regions.

is also a true nanofabrication technique where 22 nm wide individual lines written in hydrogen silsequioxane have been demonstrated [vanK06]. This method is therefore very suitable for production of 3D cell-growth substrates with nanoscale features.

In an alternative approach, rather than focusing the MeV ion beam and scanning it across the resist, the target is moved relative to a small beam spot defined by an aperture [Tayl06, Tayl07] or a set of apertures [Volc2000, vanE06].

The major drawback in using focused (or collimated) beam writing is its slow exposure speed since the patterns are exposed serially, pixel by pixel. Exposing the large areas that are required in biomedical research may therefore be very time consuming. In an alternative approach developed in Jyväskylä, a rectangular beam spot is defined by a computer-controlled variable size aperture placed in close proximity to the sample [Paper III]. By moving the sample relative to the beam spot and by changing the beam spot size by altering the aperture opening, entire patterns made up off rectangular elements can be exposed in short time (Fig. 1.1).
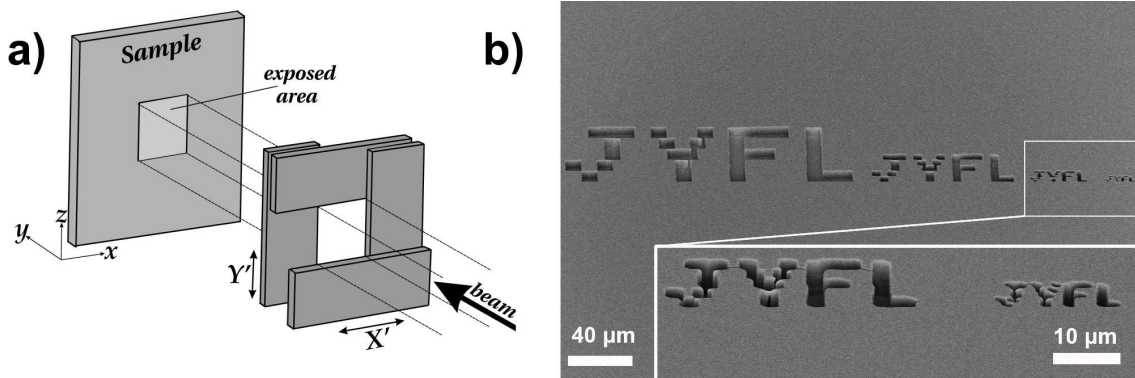
Figure 1.1: Schematic illustration of the PPAL principle. a) Two L-shaped aperture blades, each made up of two Ta sheets glued together, define the beam spot shape and size on the sample. By combining movement of the sample with different aperture openings, entire patterns made up off rectangular structures can be exposed. b) Example of an exposed pattern combining both large and small structures on the same sample written during the same exposure. The written pattern reproduces the acronym of the Physics Department of the University of Jyväskylä (Jyväskylän Yliopiston Fysiikan Laitos - JYFL) in 7.5 μm thick PMMA on a Si substrate. The JYFL patterns were written using 3 MeV ^{4}He^{2+} beam from the Pelletron accelerator.

This method, namely Programmable Proximity Aperture Lithography (PPAL), is considerably faster than the P-beam writing because entire pattern elements, rather than being written pixel-by-pixel, are written in one exposure. The exposure time per pattern element is determined by the beam current density and does not depend on the pattern size. This means that both large and small structures can be easily combined in the same pattern (Fig. 1.1b), whereas exposure of large pattern elements

with a focused beam requires either long exposure times or a second exposure step with a defocussed beam. The PPAL is thus very suitable for writing microfluidic devices which combine large and small elements for a large variety of applications, including cellular studies.

As the PPAL approach is purely based on beam shadowcasting, it can be used with beams that are hard to focus, e.g. MeV heavy ion beams or beams having large divergence. The damage produced by heavy ions along their penetration trajectories can be etched away thus producing single ion-tracks which have diameters of only a few tens of nm. The PPAL system can thus be used to define areas of such ion tracks. The areas containing overlapping ion-tracks form regions with nanometre features which can be used as substrates for biomimetic studies to probe the influence of chemical signalling combined with nanometre-scale topography on cell proliferation.

Theoretical investigations indicate that the PPAL system can be used to produce sub-100 nm structures. Indeed, some of the recent experimental results presented in this thesis show that the system has real potential for nanofabrication.

The experimental part of this thesis is focused on the development of MeV ion beam micro- and nanofabrication for bio-applications. The theoretical part deals with the MeV ion scattering from the aperture edges which may present a limitation on the resolution of the PPAL system.

1.2 Structure of this study

A brief overview of the physics of ion-matter interactions is given in Chapter 2. The destructive or constructive changes induced by the ions penetrating through matter can be employed to structure materials on a fine scale using lithography methods. The basics of the microfabrication and lithography are discussed in the same chapter.

A description of the experimental facilities is presented in Chapter 3. Here, we briefly describe the nuclear microprobe facility at the Centre for Ion Beam Applications (CIBA), National University of Singapore, where focused proton beam work was carried out. The design of the PPAL system in Jyväskylä is discussed in a more detail.

Applications of a focused proton beam for production of cell-growth substrates for culturing osteoblasts (bone-forming cells) and adhesion of high aspect ratio nanostructures to different substrates are presented in Chapter 4. The same chapter also presents applications of the PPAL system in manufacturing of microfluidic devices. Using the PPAL system, sub-micrometre structures in thick resist films were realized. The results indicate that the sub-100 nm resolution is achievable. Defined regions of

ion-tracks are formed when low fluences of heavy ions are used for irradation of resists. Increasing the fluence results in overlapping of the ion-tracks and formation of regions having nanometre texture. Possible applications of such defined regions of overlapping ion-tracks are also discussed in this chapter.

Chapter 5 discusses investigations of MeV ion scattering from aperture edges using Monte Carlo methods. The study concentrates on the scattering from a rectangular edge of a tantalum plate, from the programmable proximity aperture made up from four Ta plates, and scattering from a round edge of a tungsten carbide (WC) cylinder which is used as a beam defining slit in nuclear microscopes and the PBW system in Singapore.

Final conclusions and future aspects of the MeV ion beam lithography are given in Chapter 6.

2 Principles of MeV ion beam lithography

This section introduces the central concepts on the physics of MeV ion beams in matter. The processes associated with the penetrating MeV ions, e.g. localised damage and material modification, can be utilised as a constructive force to shape three-dimensional micro- and nanostructures in materials.

2.1 MeV ion interaction with matter

An energetic ion that penetrates a medium interacts with the target atoms. It collides with the nuclei and electrons of the target material and transfers to them its kinetic energy. The ion undergoes multiple collisions both with electrons and the nuclei, losing kinetic energy until it comes to rest at some depth inside the material bulk. The average penetration distance of a particular ion having energy E is termed the *range* of the ion. If the material thickness is smaller than the ion's range, the ion is usually transmitted through the material, losing only a fraction ΔE of its total energy E.

The energy loss of the ion, $S = -(dE/dx)$, is commonly referred to as the *stopping force*[1], that is the energy loss per unit length along the penetration trajectory. It can be divided into two separate and nearly independent components: nuclear stopping and electronic stopping. Hence, the total stopping force can be written as a sum of these two components:

$$\left(\frac{dE}{dx}\right)_{tot} = \left(\frac{dE}{dx}\right)_{nuclear} + \left(\frac{dE}{dx}\right)_{electronic} \tag{2.1}$$

For high energies (>10 MeV/nucleon) the contribution to the energy loss from nuclear reactions, relativistic corrections and bremsstrahlung (radiation emission produced by accelerating charged particles) have to be taken into account, however, for the energies considered in our work (<4 MeV/nucleon) they can be neglected.

---

[1] Other terms, such as stopping power or linear energy transfer, may be found in the literature.

2.1.1 Nuclear stopping

Nuclear stopping is the transfer of energy to target atom nuclei in elastic collisions. The nuclear stopping has a maximum at relatively low energies, of the order of 1 keV/nucleon, and it rapidly decreases as the ion energy increases. The nuclear stopping thus constitutes only a small fraction of the total stopping force exerted on the penetrating MeV ion. However, as the ion penetrates deeper into the material, its kinetic energy decreases and the contribution of the nuclear stopping to the total stopping starts to grow. Close to the end of the range, the nuclear stopping dominates the stopping process. The atoms of the material receive sufficient kinetic energies when struck by the penetrating ion to be displaced from their atomic sites generating collision cascades and inducing structural damage of the material. Most of the structural damage in the material is therefore confined to the end of the ion-range (inside the so-called "Bragg peak").

2.1.2 Multiple scattering

Nuclear stopping and scattering are closely related processes. An elastic collision of the ion with a target nucleus results in an energy loss and a small-angle deflection of the ion from its original trajectory. Multiple nuclear collisions lead therefore to the lateral broadening of a beam transversing through a material. Early theoretical work on small-angle scattering has been summarised by Scott [Scot63]. To meet the needs of experiments, the theory was further developed by Sigmund and co-workers in a series of papers [Sigm74, Marw75, Sigm78]. An example of a detailed implementation of the theory in calculations of the lateral spread of 2.1 MeV protons in biological tissues can be found in ref. [Min07]. The multiple scattering theory has recently been revised and extended by Amsel and co-workers [Amse03].

In addition to the analytical methods, the multiple scattering and energy loss can be modelled using computational algorithms based on Monte Carlo techniques. In such computer simulations, an ion undergoes a number of successive collisions with the target atoms. Typically, the collisions are treated as binary, i.e. the ion interacts with only one atom at a time neglecting the rest of the environment. Each collision results in a change of the ion's direction, energy, charge state, etc. The procedure is continued until a stop-condition is met, e.g. when the ion penetrated through a thin layer of material or when the ion has lost all its energy and stopped inside the material. Statistically significant results for various values (e.g. ion range, lateral spread, energy loss, etc.) can be obtained by simulating a large number of penetrating ions. There are several codes available, of which the most popular is SRIM [Zieg] which allows tracking of ions in layers of materials. The GEANT4 simulation toolkit [Agos03, Alli06] allows tracking of ions in complex three-dimensional geometries. In GEANT4, rather than

calculating the effect of each collision, the ion trajectory is divided into segments and the global effects (e.g. net displacement, energy loss, change of direction) of a number of collisions is calculated at the end of each segment. The multiple scattering model in GEANT4 is based on Lewis' theory [Lewi50] and uses model functions to determine the angular and spatial distributions after each track segment [GeantPhys].

2.1.3 Electronic stopping

Electronic stopping is a common term for the energy loss caused by all electronic processes that introduce changes to the ion's energy. It involves several different contributions. Some of the possible phenomena contributing to the electronic stopping in the non-relativistic velocities region are:

- Momentum exchange in a collision between the ion and an electron in the target material

- Electron capture/loss by the ion or target atoms

- Ionisation of the ion or target atoms

- Excitation of the ion or target atoms

- Collective excitation effects (polarisation, plasmon or phonon excitation, etc.)

In particular, the electronic stopping processes lead to the generation of excited electrons by ion-electron scattering. This scattering can excite electrons on both the projectile and the target atoms either to unfilled bound states or to free states. For quasi-classical scattering, the energy of the scattered free electron is $E_f = T - E_b$, where $T \approx E \cdot (4m_e/M_1) \cos^2 \varphi$ is the energy transferred to a free electron in a classical ion-electron collision with an ion mass M_1, E_b the electron binding energy, and φ is the laboratory frame scattering angle. For valence electrons, E_b is of the order of a few eV and, to a good approximation, such electrons can be considered free classical electrons ($E_b = 0$). The primary electrons (δ-electrons) from classical collisions will then have energies extending from zero ($\varphi = \pi/2$) to a maximum T_{max} at $\varphi = 0$. The δ-electrons undergo elastic and inelastic scattering with the target electrons as they move though the target material. In the scattering process the δ-electrons transfer kinetic energy to the target electrons resulting in a cascade of secondary electrons. Since the cross-section for the along-track scattering ($\varphi = 0$) is extremely small, most of the primary δ-electrons are scattered to large angles and have low energies (typically less than 100 eV [Whit04, Helb05]). These δ-electrons have only a short range, hence the electron cascade spreads to only a limited range in the material [Cham07]. This results in sharp localisation of the deposited energy within just a few nm around the ion

track where 90% of the electron energy is deposited [Wali86]. The energy deposited in the e^--e^- scattering process can lead to localised modification of the material, e.g. by breaking and forming chemical bonds in the material around the ion track.

2.2 Microfabrication and lithography

The ability of irradiation to selectively alter chemical properties of materials is utilised in microfabrication. Microfabrication (also lithography, micromachining or micromanufacturing) refers to the set of technological processes used for fabrication of devices with at least some of their dimensions in the micrometre range [Mado02]. In this section, basic microfabrication principles are described together with the associated materials and methods.

2.2.1 Basic principles

The set of microfabrication processes are summarised in the Fig. 2.1.
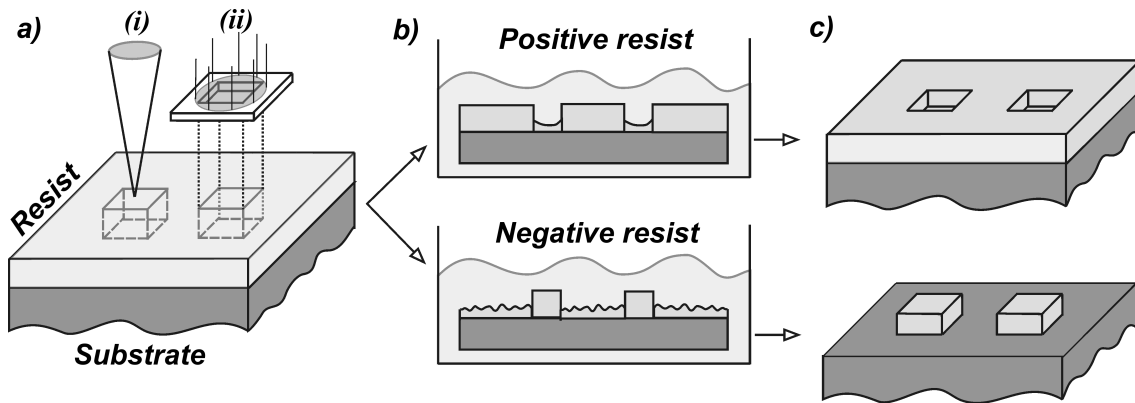
Figure 2.1: Schematic illustration of the steps in microfabrication. a) The planar substrate coated with a uniform layer of resist is exposed to irradiation. The beam of particles can be either (i) focused into a small beam spot and scanned to generate a latent pattern or (ii) the pattern can be exposed through a mask. b) The chemical changes in the resist induced by the irradiation renders the resist either soluble in the developer (positive resist) or insoluble (negative resist). c) The development process reveals the exposed pattern.

Initially, a uniform film of a polymer sensitive to irradiation is formed on a clean and flat substrate (e.g. Si wafer or glass) by spin-coating a liquid solution of the polymer followed by baking to remove the solvent. The family of irradiation-sensitive polymers

used in microfabrication are referred to as "resists". In the next stage of the processing, the sample is locally exposed to the irradiation to form a latent image of the pattern in the resist. The pattern can be transferred into the resist by means of exposure through a mask. In this case, the resist is selectively exposed by the radiation transmitted through the mask, while the "shadowed" areas remain unexposed. Alternatively, the pattern can be "written" on the resist by rastering a focused beam along a determined path transferring the pattern serially - point by point.

The latent pattern is brought forth by "development", e.g. by the sample immersion into an appropriate solution, "developer". The developer selectively dissolves away the exposed areas of the resist (for a "positive"-tone resist) or unexposed areas (for a "negative"-tone resist). The remaining resist, after a drying step, forms a 3D polymeric pattern on the substrate.

2.2.2 Positive-tone resist: PMMA

Poly(methylmethacrylate) or PMMA (Fig. 2.2) is one of the most commonly used organic positive-tone resist in microfabrication. The exposure (with Deep-UV light, X-rays, keV electron beam or MeV ions) breaks the long polymer chain into fragments in a process known as chain-scission.
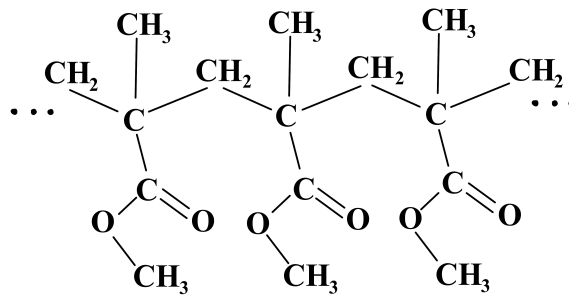
Figure 2.2: Schematic illustration of the molecular structure of PMMA.

These lower molecular weight polymer fragments are subsequently dissolved preferentially by a developer. The developer used to resolve the exposed patterns in PMMA is a mixture of propan-2-ol (IPA) with water (7:3 ratio by volume). This developer has a low viscosity, therefore, it can easily penetrate into the micro- and nanostructures efficiently resolving the pattern's features [Yasi02]. More details on PMMA patterning procedures can be found in Appendix A.

2.2.3   Negative-tone resist: HSQ

Hydrogen silsequioxane (HSQ) is an inorganic Si-based polymer which acts as a high resolution negative tone resist [Nama98]. The exposure breaks Si-H bonds and stimulates the reorganization of the Si-O bonds which leads to formation of a dense three-dimensional cage-like structure (Fig. 2.3). The structure of the exposed HSQ is similar to SiO_2 and thus it is mechanically rigid and has high resistance to solvents. The immersion of the exposed HSQ samples in 2.38% tetramethyl ammonium hydroxide (TMAH) solution removes the unexposed resist. More details on HSQ patterning procedures can be found in Appendix B.
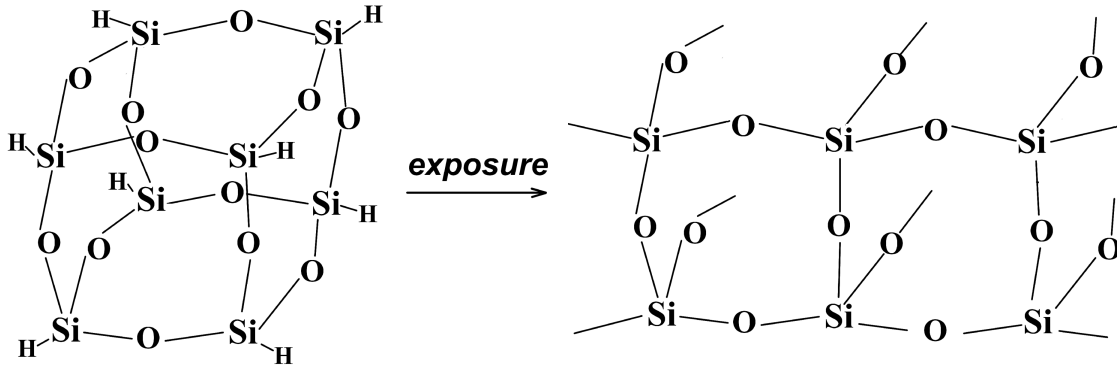

Figure 2.3: Schematic illustration of the molecular structure of HSQ. Exposure breaks Si-H bonds, and HSQ reorganizes into a three-dimensional cage-like structure [Nama98].

2.2.4   Clearing fluence

The *clearing fluence* is a minimal fluence that must be delivered onto the resist in order to render it completely soluble (for a positive-tone resist) or insoluble (for a negative-tone resist) in the appropriate developer. An exposure with a fluence smaller than the clearing fluence, i.e. underexposure, results in partial removal of the exposed positive-tone resist with the average thickness of the resist dropping with a finite slope with decreasing fluences. For D_1 the largest fluence at which no film is lost and for D_2 the clearing fluence, the contrast of the resist is defined by a following relation,

$$\gamma = \left| log_{10}\left(\frac{D_2}{D_1}\right)^{-1} \right| \tag{2.2}$$

The same expression defines the contrast of a negative resist (the film is retained where irradiated). A higher contrast resist will usually have a wider process latitude as well as more vertical sidewall profiles.

Typically, there is a range of fluences for the resist exposure. Exceeding a certain maximum, i.e. overexposing, results in a different behaviour of the resist. For instance, the positive-tone resist, PMMA, is cross-linked by overexposure which makes it insoluble in the developer. For negative resists, overexposure typically results in a significant broadening of the exposed patterns.

2.3 Advantages of MeV ion beam lithography

Apart from at the end of the range, a MeV ion interacts mostly with the electrons of the resist material along its penetration track. Because of the large mass differences between the ion and the electrons (a proton, the lightest ion, is about 1800 times heavier than an electron), the collisions of a swift ion with electrons do not result in a significant deviation of the ion from its original trajectory. This offers an advantage over keV electron beam lithography which is limited to thin resist layers (<1 μm) due to the large angle scattering of electrons in electron-electron collisions that causes significant lateral broadening of the dose around the exposed areas [Watt07]. Furthermore, the energy deposition of the MeV ions is relatively uniform with the penetration depth (apart from the end of the range where the stopping force is several-fold larger). This feature offers an advantage over conventional UV or X-ray lithographies, where the exposure exponentially decreases with depth.

The small lateral dose spreading around the ion track combined with a straight path and deep penetration depths, make MeV ions superior for fabrication of structures in thick resist films and having high aspect ratios (i.e. ratio between the height of a structure to its width).

The most common form of Ion Beam Micromachining, Proton Beam Writing [Watt07], is conceptually similar to the conventional electron beam lithography and the FIB (Focused Ion Beam) technique. A beam of MeV protons from an electrostatic accelerator is magnetically focused into a small beam spot which is then scanned across the resist (in a manner very similar to writing, hence the name "P-beam writing"). Using a triplet of quadrupole magnetic lenses, a beam of protons can be focused down to very small beam spots (<50 nm [vanK05]). The ability to produce small beam spots of MeV protons combined with their unique physical properties is very suitable for realizing 3D nanostructures with very high aspect ratios [vanK07a]. Nanostructures with aspect ratio >150 were demonstrated in SU–8 material [Watt05, vanK07a]).

The focusing of the ion beams using quadrupole magnets requires high brightness beams of high stability. In addition, focusing of heavy ion beams (heavier than He) is complicated because of their high magnetic rigidity. It is therefore not straightforward to use heavy ion beams or beams from cyclotrons that typically have large divergence.

In these cases, to generate lithographic patterns the beams are collimated by an aperture or a set of apertures, and the sample is rastered relative to the stationary beam spot [Volc2000, vanE06, Tayl06, Tayl07].

The major drawback of a focused (or collimated) beam writing is its slow exposure speed since the patterns are exposed serially, pixel by pixel. Exposing large patterns can be therefore time consuming. To overcome this drawback we have developed at the Jyväskylä Accelerator Laboratory an alternative approach, namely Programmable Proximity Aperture Lithography [Paper III, Paper IV]. In this method, a rectangular beam spot is defined by a computer-controlled *variable-size* aperture (Fig. 1.1a). Whole rectangular pattern elements can be then written in a single exposure. The PPAL method is therefore intermediate in speed between serial focused beam exposure and truely parallel exposure through a mask. The writing speed in the PPAL method is independent of the pattern size, but depends on the beam current density and the total number of pattern elements. This means that both large and small structures can be combined on the same sample (Fig. 1.1b), which coupled with its direct writing nature makes this method very suitable for fast prototyping. In addition, since the beam spot is shaped by an aperture, there are no restrictions in using heavy ion beams, highly divergent beams or beams having poor energy resolution. Using heavy ion beams at low fluences with the PPAL system offers a number of exciting possibilities, among them writing geometrically defined regions of ion tracks.

2.4   Summary of the chapter

The penetration depth of MeV ions, their relatively straight trajectories and uniform energy deposition along the penetration track (apart from the end of the range) allows fabrication of very high aspect ratio structures in thick resists. Most commonly, a beam of light MeV ions, such as protons, is focused into a small beam spot which is scanned across the resist to generate lithographic patterns. In an alternative approach the small beam spot is defined by an aperture or a set of apertures and the sample is rastered relative to the stationary beam spot. Because the ions can be focused or shaped down to sub-100 nm beam spots, MeV ion beam lithography is suitable for direct writing of nanostructures and prototype patterns. The direct writing methods, however, suffer from relatively low production speed. In the approach developed in Jyväskylä, namely PPAL, the variable-size rectangular beam spot on the sample is defined by a computer-controlled aperture. This methods is intermediate in speed between the direct writing and mask-exposure methods and can be used for fast prototyping of cell-growth substrates and microfluidic devices. Being based purely on beam shadow casting, the PPAL system can be used with heavy ions and with beams that are highly divergent or have a low energy resolution. Using heavy ions, defined regions of ion tracks containing nanometre features can be easily written which can be used as cell growth substrates.

3 Experimental facilities and procedures

Three different accelerators provided the MeV ions used in this thesis for lithographic exposures: proton beams from a single-ended electrostatic machine were focused and used to produce nanostructures; broad beams of N and He ions produced by the Jyväskylä cyclotron and a tandem electrostatic accelerator, respectively, were used with the PPAL system. The next chapters overview the components of the equipment and the lithographic exposure procedures.

3.1 Proton beam writing with a focused beam

The heart of the set-up ("a nuclear microprobe") used for production of well-focused proton beams at the Centre for Ion Beam Applications, National University of Singapore, consists of a 3.5 MV High Voltage Engineering Europa Singletron^{TM} accelerator with an associated RF positive ion source. The accelerated ions are analysed by a 90° magnet which is used to select the ions with a defined energy, which are then incident onto object slits which define the beam size. The beam is then directed by a switching magnet into the lithography beam line (10° beam line) where it is further collimated by a second set of slits that define the beam divergence. Finally, the beam is focused by a triplet of quadrupole magnetic lenses (Oxford microbeams LTD [Oxfo]) into the lithography chamber. The beam can then be scanned by means of magnetic or electric fields to write patterns into resists. More detail on the P-beam writing facility can be found in Ref. [Min07, vanK03, vanK04, Bett05].

3.1.1 Exposure parameters

In order to ensure proper exposure, it is necessary to deliver the correct fluences when writing the patterns on the resist. Thus, it is essential to measure the beam current. The currents of a finely focused beam are typically low (<1 pA) and are, therefore, very hard to measure directly.

Individual ions can be counted using a p-i-n diode. Such a diode, however, is not able

to count the individual ions if the count rate is exceeds $\sim 10^4$ ions sec^{-1}. To measure the beam current for a finely focused beam spot ($<$200 nm) of ions (e.g. protons) which may exceed 10^6 ions sec^{-1}, the p-i-n diode-SE (secondary electrons) emission calibration method is used [Bett02]. In this method, to decrease the number of ions incident on the p-i-n diode below the acceptable level of $<10^4$ ions sec^{-1} which can be measured with the p-i-n diode, the object slits are closed nearly completely to reduce the ion count rate. The same low current beam is then directed on a quartz plate, and the secondary electrons ejected from the quartz plate are detected by a Channel Electron Multiplier (CEM). The conversion ratio between the ion count rate and the count rate of the secondary electrons, R, is governed by the properties of the quartz plate at the irradiated spot and the bias voltage used to collect the secondary electrons. Setting the object slits to the required opening typically increases the ion count rate which increases the count rate of the secondary electrons. By measuring the increased count rate of the secondary electrons and scaling it using the previously obtained conversion ratio R, the count rate of ions can be estimated. The procedure is typically repeated several times for verification.

For larger beam spots, larger beam currents are available and other methods of optimisation of the exposure fluences can be used, e.g. RBS calibration [Bett02], ion induced photoluminescence [Cham03] or direct beam current measurements from the exposed sample.

Once the exposure parameters are found, digitised files containing information about the patterns to be written are loaded into specialised software, *Ionutils* [Bett05], which performs automated exposures.

3.2   MeV ion beam Programmable Proximity Aperture Lithography (PPAL)

Using the PPAL system, beams which are very hard to focus (e.g. heavy ions and beams with large divergence) can be shaped into small beam spots. The aperture in the PPAL system (Fig. 1.1a) is made up of four 100 μm thick Ta plates with well-polished edges. The maximum ion energy that can be used with the system is set by the thickness of the apertures, e.g. $<$6 MeV/amu [Paper III], when ions are completely stopped by a Ta sheet. Two sheets are glued together with a vacuum compatible epoxy adhesive at right angle to form a L-shaped blade (Fig. 3.1). Each L-shaped blade is then glued to a corresponding Al block which is mounted on a high precision positioner (Newport MFA-CCV6 DC vacuum compatible servo-motor driven linear-motion drive). By moving the lower block in the X-direction and the upper block in the Y-direction, the aperture opening size can be defined (Fig. 3.2a,b). The sample
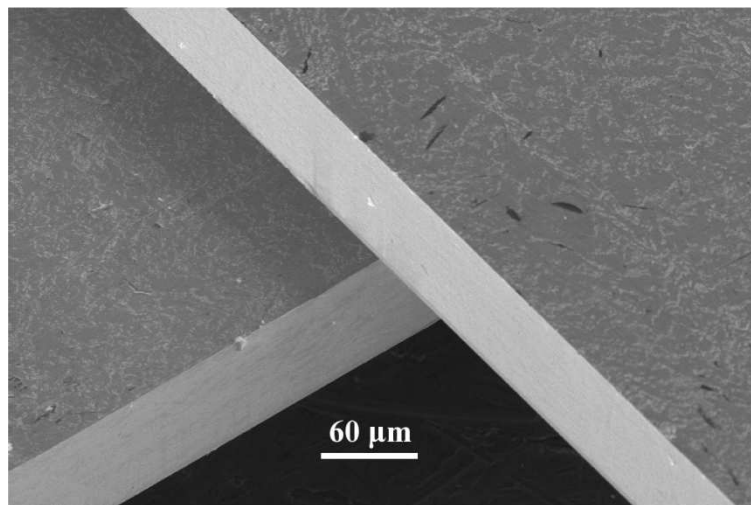
Figure 3.1: Two Ta sheets with well polished edges are glued together at right angle to form a sigle L-shaped blade.

holder is mounted on three similar positioners which can move the sample in the x, y and z directions. A fluorescent screen on one of the aluminium blocks that support the aperture L-blades is used for optimising and focusing the beam to about a few mm in diameter. A purpose-developed LabView^{TM}-based software is used to control the motion of the positioners, beam blanking and perform automated exposures by reading ASCII files containing pattern information (see Appendix C).

The lithography chamber in Jyväskylä can be mounted on different supporting frames in order to accommodate different beam heights of different accelerators. This allows a wide range of ion species and energies. The chamber can be moved between different accelerators (e.g. JYFL cyclotron and JYFL Pelletron) or even to another laboratory, albeit at the expense of realignment of the beam line at the new accelerator.

3.2.1 Jyväskylä cyclotron

The PPAL system performance was initially tested at the JYFL cyclotron. The JYFL cyclotron consists of two hollow D-shaped electrodes between which a high frequency accelerating electric field is applied. The ions are injected into the centre of the D-electrodes with an initial speed. A uniform magnetic field perpendicular to the planes of the D-electrodes bends the ion trajectory such that they start cycling in hollow space inside the D's. The alternating electric field is tuned in such a way that every time the ion passes the gap its kinetic energy is increased. The cyclic radius of the ion increases every time it passes the gap resulting in a spiral-like trajectory towards the outer edges of the D's, where the ion is extracted and transported into a beam line. The JYFL
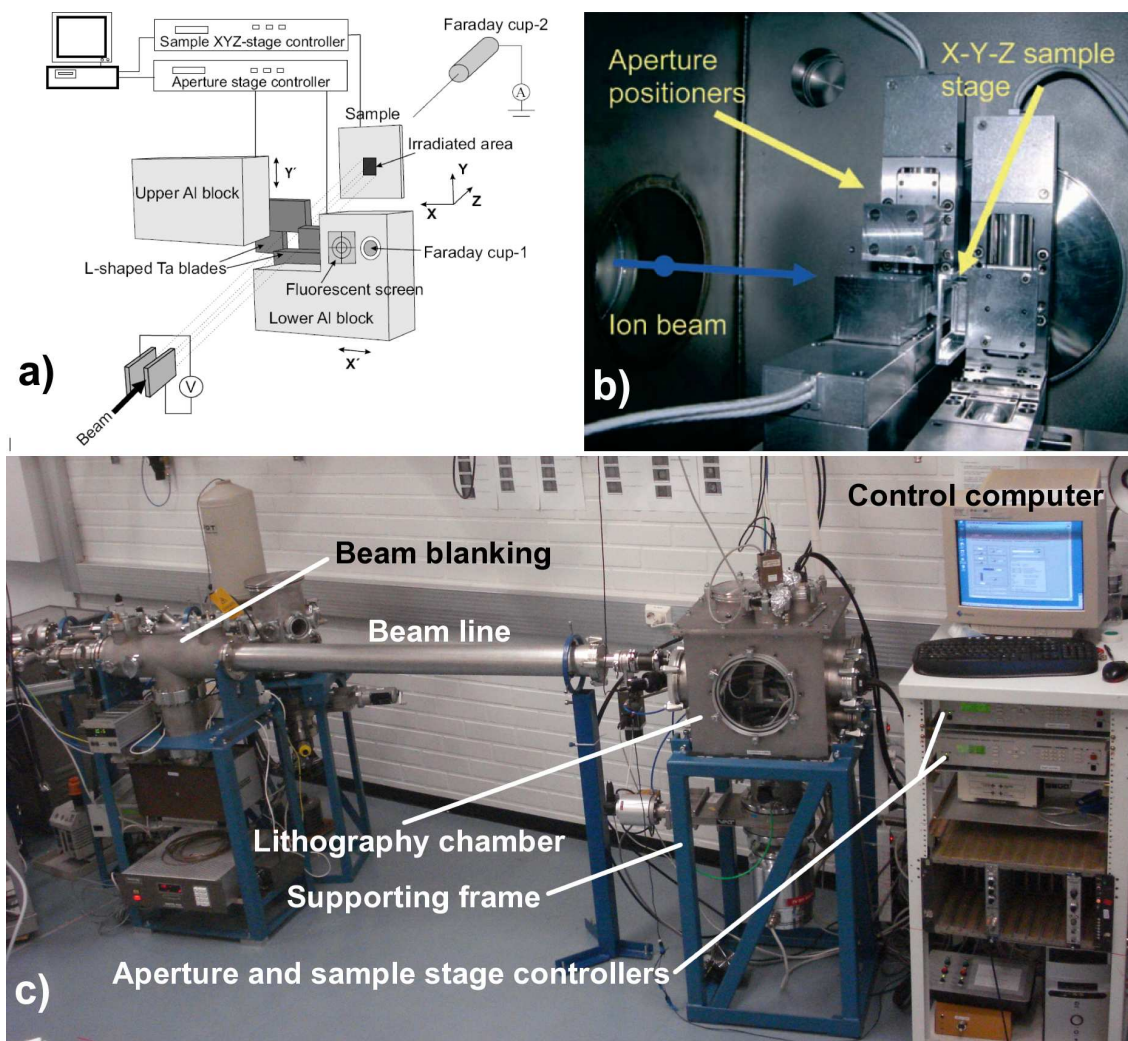
Figure 3.2: The PPAL system. a) Schematic presentation of the operational principle of the PPAL system. b) A photograph of the interiors of the PPAL chamber. The Al block are mounted on high precision computer-controlled linear-motion drives that move the L-shaped Ta blades. (Image courtesy of Timo Sajavaara). c) The PPAL system at the Pelletron laboratory.

cyclotron is equipped with a number of ion sources which facilitates production of about 100 different ion species that can be accelerated up to the $130A/q^2$ MeV, where A is the ion atomic mass number and q is its charge state as it enters the cyclotron. The beam blanking is achieved by sending a TTL signal to the accelerator injection system which stops ion injection into the cyclotron. More detail on the cyclotron can be found elsewhere [Liuk92, JYFL].

In our cyclotron tests we used a beam of 56 MeV $^{14}N^{3+}$ ions since sufficient beam currents of this ion species can be obtained relatively easily.

3.2.2 Tandem Pelletron accelerator

For PPAL irradiations with light ions the 1.7 MeV Tandem Pelletron accelerator (National Electrostatic Corporation) in Jyväskylä was used. This accelerator is equipped with an RF ion source (Alphatross) which generates negative ions of H or He. These negative ions are preaccelerated to a few 10's of keV energy, δE, and a beam shaped by a Wien velocity selector and an Einzel lens is injected into the accelerator. The negatively charged ions are accelerated towards the centre of the accelerator tank by the attractive force of the positively charged terminal. In the centre they pass through a *stripper*, a tube filled with low pressure N_2 gas. In collisions with the N_2 molecules, most of the ions are ionised rendering them positively charged. These positive ions are then repelled by the positively charged terminal in the second acceleration stage (hence the "tandem" name of the accelerator) towards the ground potential. The total kinetic energy acquired by the ion is therefore $E = (1 + q)V + \delta E$ (MeV), where V is the terminal voltage in MV, q is the charge state of the positive ion. The protons can therefore be accelerated to $E = 2V + \delta E$. Other ions may form several charge states after they pass through the stripper, e.g. He will form He^+ and He^{++}. For the same acceleration voltage V, the He ions are accelerated to two different energies: $E = 2V + \delta E$ and $E = 3V + \delta E$ for He^+ and He^{++}, respectively. The required energy is filtered by the switching magnet which diverts the beam with the selected energy into the lithography beam line ($-15°$). Beam blanking is achieved by biasing a pair of 20 cm long plates, separated by 5 mm with a potential difference of 3 kV delivered via a high voltage relay. The relay is controlled by TTL signals delivered from the control computer via a PCIe-6251 multifunction DAQ card (National Instruments). Fig. 3.2c shows the PPAL system in the Pelletron lab.

3.2.3 Exposure parameters

The experimentally determined optimal fluence of 2 MeV protons for PMMA exposure is 1 proton nm^{-2} (10^{14} protons cm^{-2}) [vanK99]. For heavy ions (e.g. 3 MeV He and
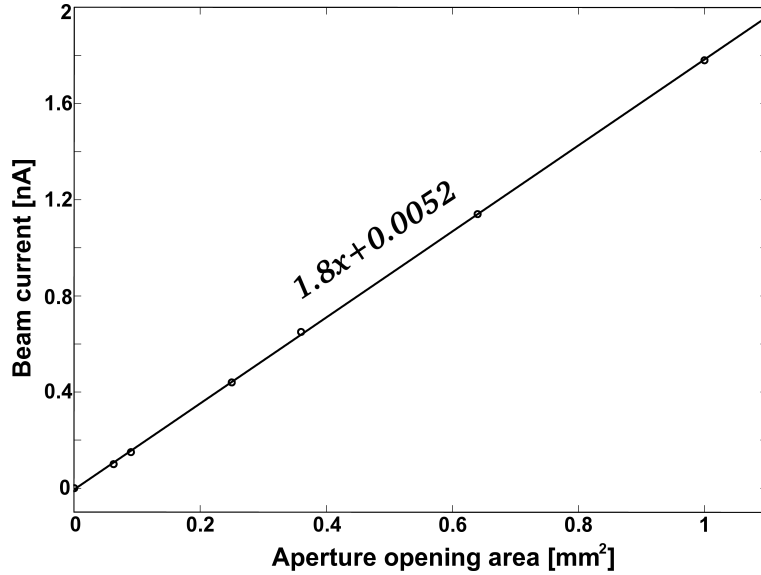
Figure 3.3: Measurement of the beam current transmitted through different size of the aperture opening. The slope of the linear fit is the beam current density.

56 MeV N ions) the required fluences can be estimated by taking into account the differences between the stopping force of the heavy ion and 2 MeV proton. For instance, the stopping force of 2 MeV proton in PMMA is 16.2 eV nm^{-1} while for 3 MeV He it is 126 eV nm^{-1}, and 442 eV nm^{-1} for 56 MeV N [Zieg]. The difference between the stopping forces suggests that the required fluence of 3 MeV He and 56 MeV N is 1.3×10^{13} ions cm^{-2} and 3.6×10^{12} ions cm^{-2}, respectively. These values can be further verified experimentally by writing a series of lines in the resist with varying fluences which values span a several orders of magnitude around the theoretical estimate.

The exposure times per pattern element are then estimated from the measurements of the beam current density. The beam current density is estimated from the beam current versus the aperture opening measurement (Fig. 3.3) by means of the Faraday cup no. 2 (Fig. 3.2a). For instance, at 0.9 particle-nA mm^{-2} beam current density of 3 MeV ^{4}He^{2+} the calculated required exposure time is about 25 seconds[1], provided the beam current from the accelerator remains stable throughout the exposures. To compensate for the beam current instabilities, a typical safety factor of 50% is added to the exposure times. Once the exposure parameters are found, an ASCII file containing information about the pattern (such as relative coordinates of the structures and exposure times per pattern element, see Appendix C) can be loaded into a purpose-built LabView^{TM} software which then performs automated exposures.

---

[1] The beam current density measured with the Faraday cup is 1.8 nA mm^{-2} since each He ion carries double the elementary charge. The exposure depends only on the total number of ions over the exposure area, independent of the charge state of the ion.

4 Experimental results

In this chapter some of the test structures produced using MeV ion beam lithography are presented along with the possible applications. The lithography with MeV ions was carried out using two different exposure strategies: exposures with a focused beam and exposures through a variable-size aperture (Programmable Proximity Aperture Lithography). Both of these strategies have strengths and weaknesses and it is important to know them in order to be able to apply the strategy that is best-suited for a given application.

4.1 Lithography using a focused MeV proton beam

In this lithography method, the patterns are exposed with a focused beam of MeV protons. Since the beam can be focused down to small beam spots (sub-100 nm), this method is suitable for nanofabrication.

4.1.1 Cell-growth substrates

The tissues in organs have a three dimensional organisation which together with the chemistry of the surfaces governs the cellular behaviour in tissues. Thus, osteoblasts (bone building cells) may start to generate new bone tissue once they reach a bone fracture or narrow and long channels which might be produced by osteoclasts, cells recycling the old bone tissue. Producing such narrow and long channels artificially along with coating the surface of the structures with appropriate chemicals to reproduce the chemical environment found in the real bone tissue can trigger the osteoblasts to start generating new bone tissue *in vitro*. The generated artificial bone tissue could potentially be later incorporated into the body. Therefore, having the information on how different three dimensional surface geometry influences the cellular behaviour is crucial for the success of tissue engineering.

Using MeV ion beam lithography three dimensional structures can be produced on artificial cell-growth substrates and the cellular response to different topological constrains on the substrates can be studied. Ions focused into small beam spots can be used to expose thick photoresists to produce deep and long channels with various

widths. In a preliminary study of the osteoblast growth on artificial cell growth substrates, test structures made of channels were written in thick PMMA layers (10 μm) using proton beam writing [Paper I]. Prior to the PMMA layer deposition on the substrates (glass cover slips) and subsequent proton beam writing, the substrates were coated with thin layers of hydroxyapatite-like films by sputtering [Saga07]. Hydroxyapatite is an inorganic mineral which is an important constituent of bone tissue. Two different channels were written in PMMA: 10 μm and 0.4 μm wide. Since the lines were written on the same sample, a direct comparison of the cellular behaviour growing on surfaces with different geometries could be made. The cellular behaviour was found to differ significantly. It was expected that the osteoblasts would prefer growing inside the 10 μm wide channels [Rahk], since *in vivo* they are found in similar channels produced by osteoclasts, that are bone absorption and recycling cells. Furthermore, it was expected that the hydroxyapatite-like layer at the bottom of the channel would attract the osteoblasts since it is a more natural growth environment for osteoblasts, as compared with PMMA. The osteoblasts, however, were found to grow primarily on the ridges between the 10 μm wide channels with no osteoblasts inside the channels (Fig. 4.1a). In case of the 0.4 μm wide lines, the osteoblasts tended to grow above the channels extending their filobodia along and inside the channels (Fig. 4.1b).

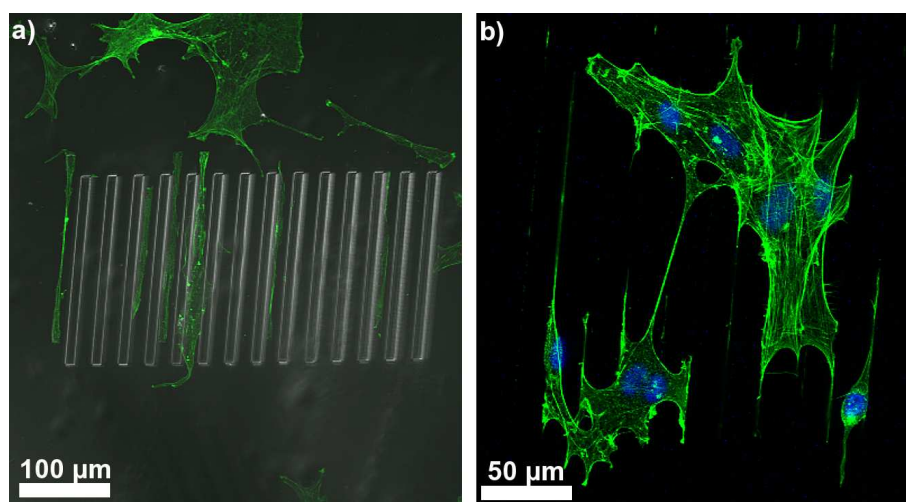**Figure 4.1**: Fluorescence confocal microscope images of murine osteoblast cells (green) cultured on PBW-machined 9 μm PMMA/50 nm sputtered-hydroxyapatite/glass substrates. a) 10 μm wide channels. The osteoblasts are aligned along the ridges in between the channels. b) 0.4 μm wide channels. Blue denotes cell nuclei. The osteoblasts extend filobodia inside and along the channels.

In both cases the cells aligned themselves in the direction of the channels or ridges with their cytoskeletons elongated along the channels or ridges. This is a sign that the cells sense the surface geometry and respond to it. The results of this study are important for understanding the response of the osteoblasts to different surface topography and chemistry, however, additional experiments are required to provide more information

on how the osteoblasts react to different geometrical constrains and environments in order to be able to guide the cell growth and trigger bone-tissue formation.

4.1.2 High aspect ratio nanostructures for nickel electroplating

In biomedical studies typically large quantities of test samples are required which contain both large and small structures covering large areas. Ion beam lithography with a focused beam is suitable for high resolution manufacturing, but as noted above suffers from a relatively low throughput. It is therefore beneficial to write one master sample which can be used to produce a negative image of the structures in a metal stamp, e.g. by Ni electroplating, and to use the metal stamp to reproduce the positive image of the patterns in polymers by replication or using nanoimprint or hot embossing technologies.

HSQ resist was found to be very suitable for producing high aspect ratio nanostructures by proton beam writing [vanK06, vanK07] or even by e-beam writing [Baek05, Tiro07] due to the high contrast properties of HSQ [Delf2000, Delf02, Word03]. In this study we investigated a possibility to use high aspect ratio HSQ nanostructures as a master for Ni electroplating [Paper II, Gore09d]. Typically, the substrate is coated with a thin Au layer (conductive seed layer) which is necessary to initiate the plating process since the conductivity of the Si wafers is insufficient. The HSQ layer can be then directly spun on the Au/Cr/Si or Au/Ti/Si substrates and the nanostructructures written in the resist. An intermediate Cr or Ti layer is used since the adhesion of Au to Si is poor. It was found that the high aspect ratio HSQ nanostructures did not adhere well to Au/Si substrates and the structures with aspect ratio greater than two were washed away from the substrate during the development process [Paper II].

In order to improve the adhesion, the Si substrates were coated with Ti or Cr layers prior to the HSQ spinning. Both Ti and Cr are highly electronegative and are commonly used as adhesion promoters. As opposed to nanostructures written on Au/Cr/Si substrates, the adhesion of HSQ nanostructures with aspect ratios as high as 15 was excellent both to Cr/Si and Ti/Si substrates. Some of the HSQ lines written with lower fluence exposures had even smaller widths. These lines were well resolved and adhered well both to Cr/Si and Ti/Si substrates, however, they were not sufficiently rigid and collapsed. Presumably, these fine lines had aspect ratios even greater than 15, but since they collapsed their widths and the aspect ratios could not be properly measured.

Unfortunately, even though the adhesion of the HSQ nanostructures was found to be excellent to Cr/Si and Ti/Si, grain-like debris was formed at the interface between

the HSQ written lines and the substrates (Fig. 4.2). The debris was more pronounced on Cr/Si compared to Ti/Si. The extent of the debris depends on the proton fluence that was used to write the line with the debris becoming thicker and extending to larger areas as the fluence is increased (Fig. 4.2b,d). No debris was observed around the lines written on Au/Cr/Si substrates which suggests that the debris was caused by a chemical reaction at the interface between Cr or Ti with HSQ.

Ni electroplating using the HSQ nanostructures on Ti/Si as a mold was realized with limited success because the debris around the lines caused deterioration of the edge quality of the Ni stamp [Paper VII, Gore09d]. Reducing the proton fluences helps to reduce the extent of debris around HSQ structures written on Ti/Si substrates, however, the lines written with low fluences tend to tilt or even collapse. Such tilted or collapsed lines cannot be used in Ni electroplating. The tilt or collapse of the lines can be prevented by using supercritical resist drying with CO_2 instead of conventional resist drying by N_2 blow that follows after-development step and rinsing in water. The supercritical CO_2 drying was shown to be suitable for production of high density, high aspect ratio HSQ nanostructures [Wahb06].
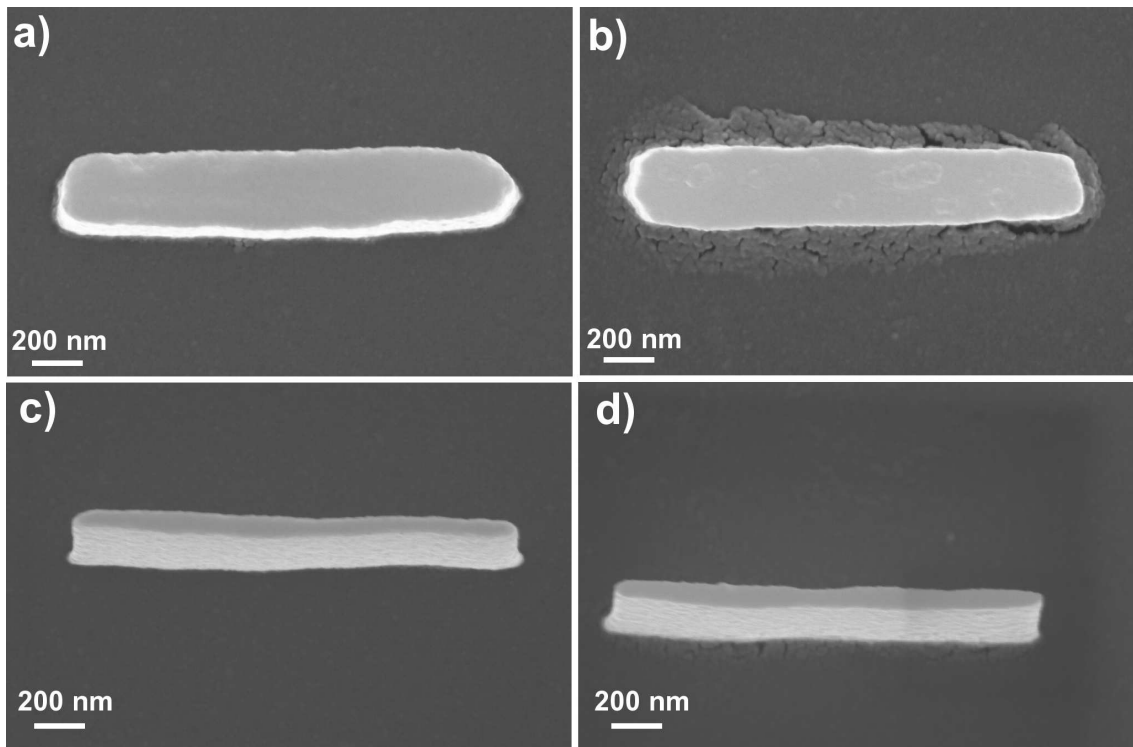

Figure 4.2: Scanning Electon Microscope (SEM) images of lines written with 2 MeV protons in 1.2 μm thick HSQ on Ti/Si and Cr/Si substrates. 17-pixels wide lines on a) Ti/Si and b) Cr/Si written with a 2.2×10^6 protons μm^{-2} fluence. 9-pixels wide lines on c) Ti/Si and d) Cr/Si written with a 2.7×10^6 protons μm^{-2} fluence.

The structures in Ni stamps fabricated by using HSQ on Cr/Si as a mold were significantly deteriorated since the extent and the thickness of the debris around the HSQ lines on Cr/Si is larger than on Ti/Si. Using Ti/Si for substrates in proton beam writing is therefore more optimal.

4.2 Programmable proximity aperture lithography

In this lithography method, the patterns are exposed through a rectangular variable-size aperture. The method is significantly faster than the PBW where the patterns are exposed pixel-by-pixel with a focused beam of ions. Furthermore, with the PPAL system no beam focusing and optimisation routines are required, and the lithography can be performed even with beams which are in general hard to focus, such as highly divergent beams, beams having poor energy resolution and beams of heavy ions. This has the drawback of a somewhat reduced resolution as compared to PBW and is limited to patterns solely made up off rectangular elements.

4.2.1 Low fluence exposure - defined regions of ion-tracks in PMMA

The damage induced by single heavy ions along their penetration tracks in PMMA – latent ion track – can be etched away in a conventional development procedure. The development yields a cylindrical void in the resist typically a few tens of nm in diameter. With the PPAL system, defined regions of non-overlapping ion-tracks can be written. Increasing the fluences leads to overlapping of the ion-tracks and formation of regions with nanometre features (e.g. nanocolumns). By varying the fluence, the size and the density of the nanostructures within the defined regions can be controlled (see Fig. 4.3 for He beam exposures and Fig. 4.4 for N beam exposures).

When the fluence value reaches the threshold, *the clearing fluence*, the ion tracks completely overlap and the exposed areas are completely developed. The experimentally found lower fluence limit for 3 MeV He is 1.7×10^{13} ions cm^{-2}. This lower limit of the fluence is in good agreement with the estimate calculated in Chapter 3, 1.3×10^{13} ions cm^{-2}, using the comparison of the stopping forces between 2 MeV protons with 3 MeV He ions and scaling the experimentally found exposure fluence of 2 MeV protons [vanK99].

The study of cell proliferation and behaviour requires large patterned areas (mm^2–cm^2). The relative ease of producing both large and small regions containing nanometre features with the PPAL system offers a possibility to produce cell-growth sub-
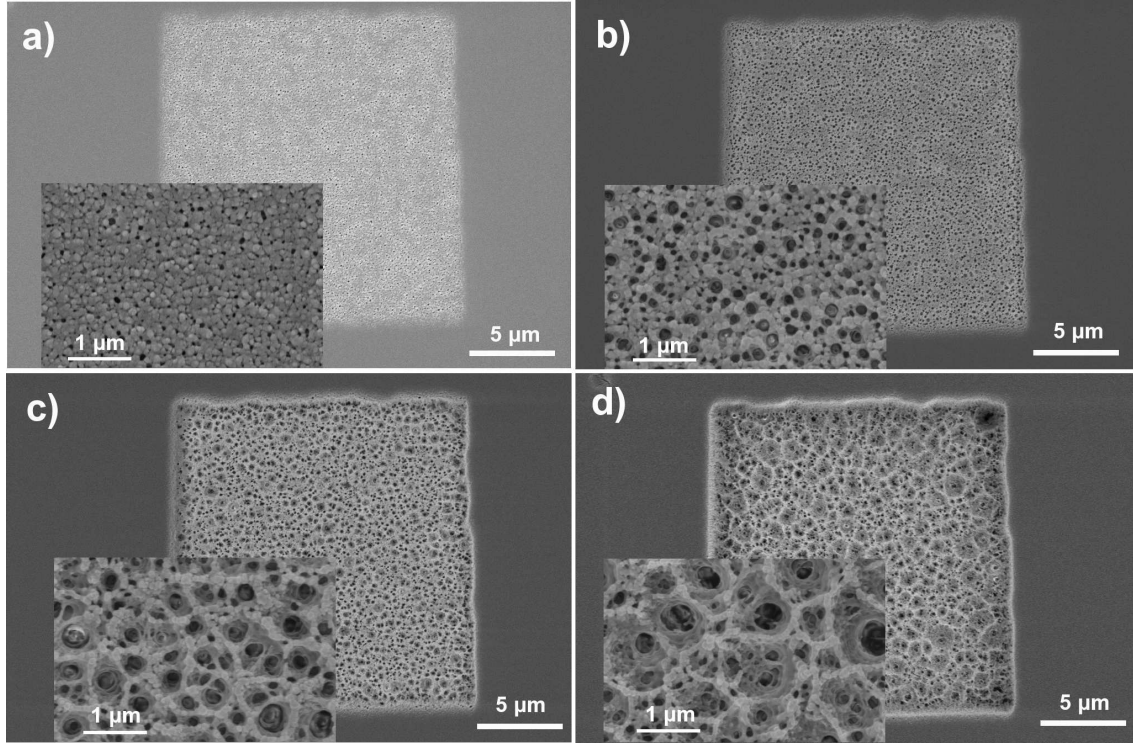
Figure 4.3: Regions of ion-tracks written in 7.5 μm thick PMMA with 3 MeV He ions from the Pelletron accelerator. a) Fluence 5.5×10^{12} ions cm^{-2}. b) Fluence 8.3×10^{12} ions cm^{-2}. c) Fluence 1.1×10^{13} ions cm^{-2}. d) Fluence 1.4×10^{13} ions cm^{-2}.

strates which can be then coated with chemical substances of interest. These substrates can be used to study the influence of chemical signalling combined with nanometre-scale topography on cell proliferation and function.

4.2.2 Fluence range for PMMA exposure with 3 MeV He ions

For the fluence range 1.7–9×10^{13} ions cm^{-2} the exposed structures are well resolved and have sharp edges. As the fluence is increased above 9×10^{13} ions cm^{-2}, PMMA starts to cross-link and cannot be dissolved by the developer, which in some applications may make the patterns unusable. This is particularly important when writing two or more overlapping structures (stitching) which is required in order to ensure that structures are properly bonded without a break between them. This is needed because of the finite setting accuracy of the positioners which gives registration errors. The need in stitching may rise for example when, in a device, two reservoirs need to be connected by a narrow flow channel. In this case, the narrow channel is designed in the pattern such that its edges extend into the reservoirs to a distance such that
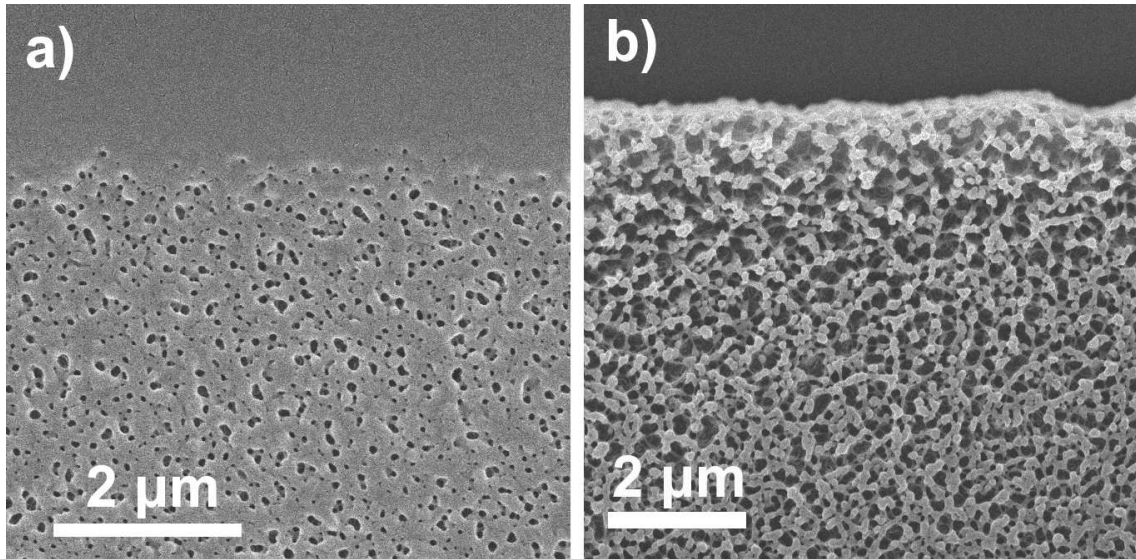
Figure 4.4: Regions of ion-tracks written in 7.5 μm thick PMMA with 56 MeV ^{14}N^{3+} ions from the JYFL cyclotron. a) Low fluence results in single non-overlapping or only partially overlapping ion tracks. b) At higher fluences, but still below the clearing fluence, the ion-tracks overlap forming a "polymer nanocarpet" - region filled with nanocolumns.

the good stitching is ensured. The overlapping areas of the narrow channel extending into the reservoirs (stitching areas) will receive double the fluence. The accumulated exposure in the stitching area therefore should not exceed the upper limit of the exposure fluence, since otherwise the crosslinked resist may block the channel (Fig. 4.5).

4.2.3 Microfabrication using the PPAL system

In the fluence range 1.7–9×10^{13} ions cm^{-2} for 3 MeV He ions, the PPAL system is useful for production of various microfluidic devices. Both large structures, such as reservoirs, and small structures, such a narrow flow channels connecting the reservoirs, can be combined on the same sample and rapidly exposed (Fig. 4.6). Fig. 4.7 shows channels of different widths written in thick PMMA with the PPAL system. The channels are well-resolved and have sharp edges. The inspection of the channels edges reveals that the edge deviations from the straightness are reproduced from channel to channel (Fig. 4.7a,b) and these may hence be attributed to the aperture edge roughness. This is discussed in more detail in Chapter 4.2.4.

The results indicate that the PPAL can be used to write rapidly narrow and wide channels with sharp edges and relatively straight walls, proving the feasibility of the approach of the PPAL system with MeV ions.
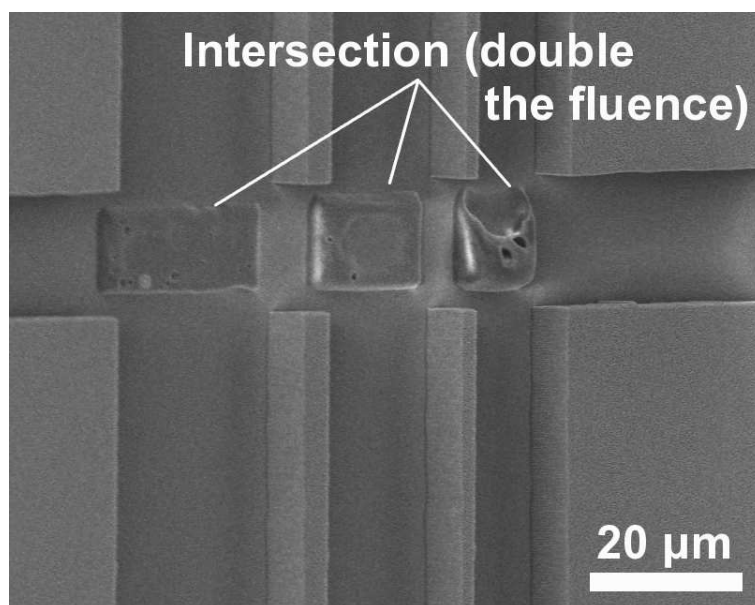
Figure 4.5: Channels written in PMMA using the PPAL system with 3 MeV He ions. The channels are intersecting, and the areas of intersection receive double the exposure fluence. The original fluence was so high that the double fluence exceeds the upper exposure limit, and hence the PMMA starts to crosslink in the intersections.

4.2.4   Resolution limit of the PPAL system

It is interesting to consider what the ultimate resolution of the PPAL system is and what factors restrict the resolution performance. Fig. 4.8 shows the smallest features written so far with the system. The smallest line in the image is only 200–400 nm wide. The edge waviness, that is exactly reproduced from line to line on a smaller scale, results from the irregularities of the aperture edge. The measured edge roughness of the aperture blades is ~100 nm [Paper III] which agrees well with the edge roughness of the exposed patterns. The restriction on the resolution imposed by the quality of the aperture edges can be addressed by improving the polishing methods, e.g. by using grazing angle sputtering [Weiss97, Laba98] or lateral smoothing by cluster-ion bombardment [Yama07]. The edge roughness of the aperture blades is thus expected to be decreased from the current 100 nm to 10 nm peak-to-valley value.

The precision of the positioners used to move the aperture blades is important for obtaining correct and reproducible aperture opening dimensions and hence the sizes of the exposed patterns. By measuring the relative distances between periodically exposed patterns and comparing these with the intended distances, the accuracy of the positioning can be determined [Paper V]. In such a measurement, the standard deviation of the distribution of the measured distances (40 nm) or the FWHM of such a distribution (100 nm) are measures of the positioning precision of the motion drives.
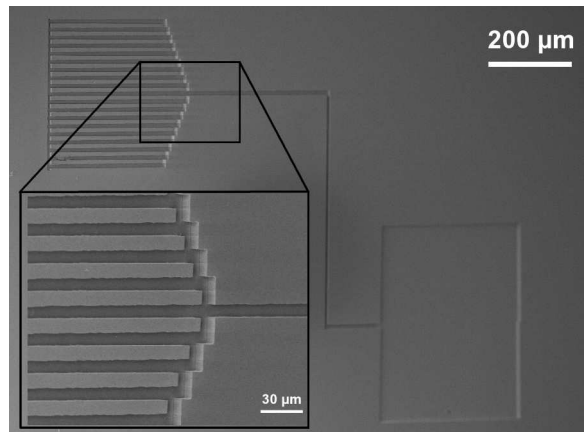
Figure 4.6: Example of an exposed pattern of a prototype microfluidic device combining a large reservior (500×500 μm) connected via a narrow flow channel to the set of capillaries (about 10 μm wide). The image tilt is 45°. (From Liping Wang, unpublished data).

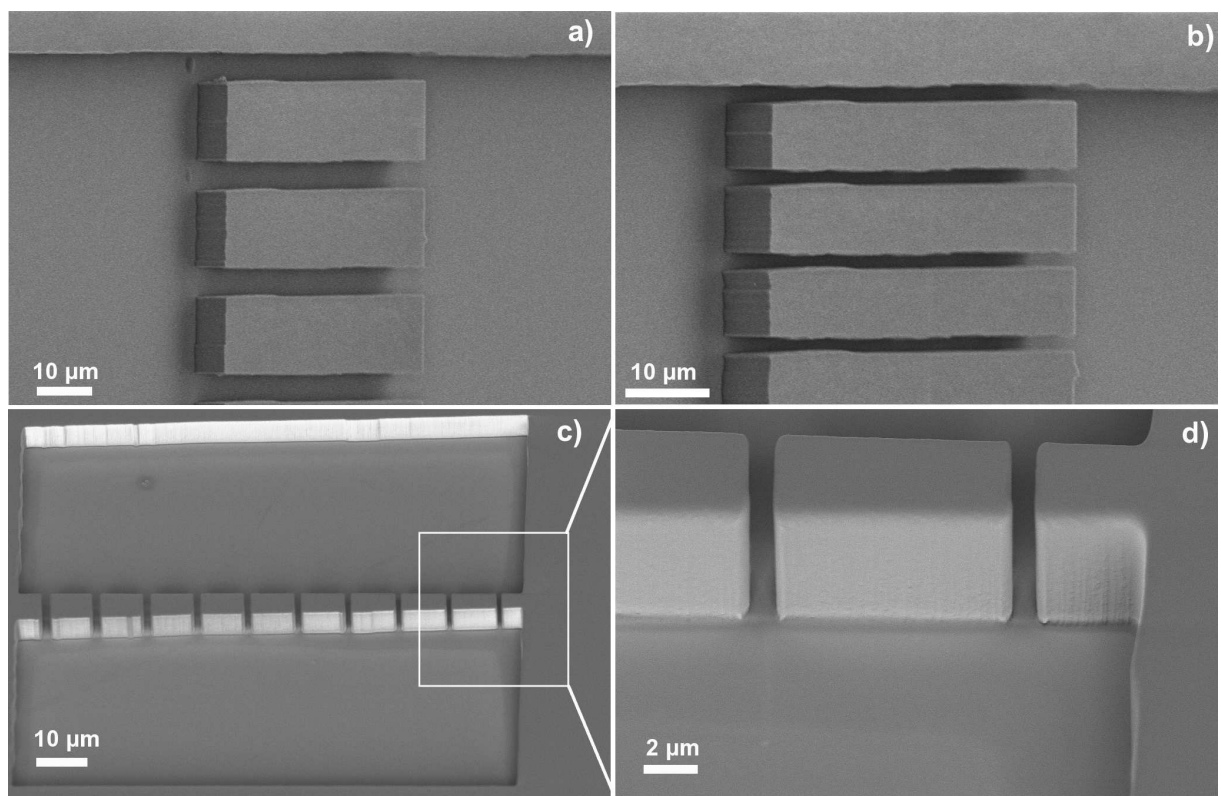**Figure 4.7**: SEM micrographs of microchannels written in 7.5 μm thick PMMA layer using the PPAL system with 3 MeV ^{4}He^{2+} beam from the Pelletron accelerator. a) 5 μm wide channels. b) 1.5 μm wide channels. c) Two reservoirs are connected with microchannels of various widths (1–2 μm). d) close-up of ~1 μm wide channels from c).
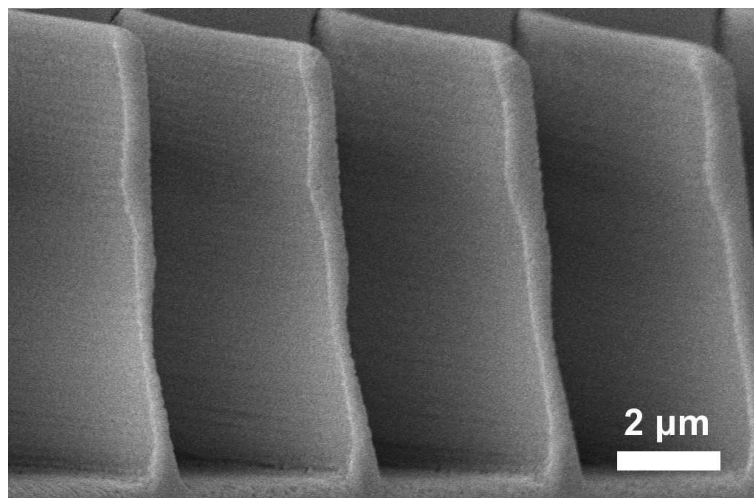
Figure 4.8: Scanning electron microscope (SEM) images of the smallest line structure written so far with the PPAL system in 7.5 μm thick PMMA with 3 MeV He ions.

This, as noted above, determines the registration accuracy. The measured accuracy is, however, comparable with the error of the measurement resulting from the uncertainties of the edge thickness of the structures of a few pixels and the uncertainty of the pixel size in the SEM images. The estimated positioning accuracy is also comparable with the manufacturer's specifications for the motion drives. Using motion drives with a better positioning accuracy can decrease the uncertainty of the positioning to <10 nm.

4.2.5 Thermal stability

The thermal stability of the system is of importance for pattern accuracy. Two issues need to be considered: (i) the size of the beam spot on the target with respect to the beam-heating-induced thermal expansion and contraction of the aperture blades and (ii) the relative position of the beam spot on the sample with respect to the thermal expansion and contraction of the components of the PPAL system.

Irradiation of the aperture with MeV ions results in a temperature increase of the aperture blades. The associated thermal expansion of the aperture blades can degrade the accuracy of the PPAL system. The heating of the aperture blades attributed to the MeV ion irradiation was not measured directly because the geometric constrains make the measurement difficult. The upper limit of the thermal expansion of the aperture blades can, however, be simply estimated. The heating power of 10 nA beam of 3 MeV $^4\text{He}^{2+}$ ions focused to a beam spot of 2 mm in diameter and impinging on the 1 mm

edge-width of the first Ta aperture blade[1] exposed to the beam (Fig. 3.2a) is 7.5 mW. Assuming one-dimensional heat flow and neglecting radiative losses, the maximum of the temperature enhancement at the thermal equilibrium was found to be 2.6 °C, giving a 20 nm associated thermal expansion of the edge width of the aperture blade[2].

When neglecting the heat conductivity from the aperture blade to the Al mounting block and attributing the heat dissipation by radiative losses only[3], the calculated maximum temperature increase of the aperture blade at the thermal equilibrium is 6.1 °C giving a 300 nm thermal expansion of the aperture blade. The cooling of the aperture blade due to the radiative losses is, therefore, less efficient than the heat conduction. The radiative losses, however, add to the cooling of the aperture blade, thus reducing the total temperature increase and the thermal expansion of the Ta blade.

Nevertheless, these estimated thermal expansions are significantly overestimated and should be treated as extreme upper limits because the beam currents are typically lower and, moreover, the beams are defocused. The actual temperature increase of the aperture blades could be measured by means of an infra-red camera mounted within the lithography chamber (Fig. 3.2b).

The thermal drifts due to the temperature fluctuations in the laboratory (<2 °C) and the differences of thermal expansion of the different materials used in the design of the PPAL system (e.g. Al and stainless steel) may result in uncertainties in the relative position of rectangular pattern elements written on the target. The upper limit of this thermal drift was estimated from a simplified design of the PPAL system (Fig. 3.2b) to be on the order of 2 μm for a 2 °C temperature difference. This is again a significant overestimation since the temperature differences during an exposure experiment are typically much lower ($\sim$50 mK or less). Furthermore, no significant deviations in the written pattern dimensions were observed over long periods of experiments, and, as mentioned above, the pattern accuracy was consistent with the motor-drive specifications. The thermal drifts associated with the differences in the thermal expansion of

---

[1]The first Ta aperture blade exposed to the beam is subjected to the maximum of the thermal load, while the blades lying further downstream experience reduced exposures due to the aperture blade mounting (Fig. 3.2a). Assuming that the 2 mm beam in diameter is perfectly aligned with the axis of an infinitesimally small opening of the aperture opening, only half of the beam current will impinge on the 1 mm edge-width of the first aperture blade exposed to the beam, and a quarter of the beam current on the second and the third blades.

[2]The rest of the aperture blade is in thermal contact with the Al mounting block through a layer of epoxy adhesive and electrical contact to prevent charging of an electrically isolated aperture blade. The heat from the exposed region of the aperture blade flowing to the rest of the blade is effectively removed through heat flow (the thermal resistance can be assumed to be typical for a transistor mounting and equal to about 0.5 K W^{-1} cm^{-2}). Hence, only the thermal expansion of the exposed edge is taken into account.

[3]Here we assume that the heat is lost through a black body radiation from the surface of a 8×13 mm Ta aperture plate.

different materials in the PPAL system are therefore very small and can be further reduced by replacing some components using materials with similar thermal expansion and installing climate control in the laboratory.

Hence the significant factors affecting the resolution of the PPAL system are the aperture edge quality and the precision of the motion drives. These resolution restricting factors can be easily addressed, and the performance of the PPAL system can be improved to reach sub-100 nm resolution. There are, however, other extrinsic and intrinsic resolution restricting factors, such as penumbra broadening due to the beam divergence, and aperture edge-scattering. These are discussed in the next chapter (Chapter 5).

4.3   Summary of the chapter

Using MeV ion beam lithography, various micro- and nanostructures, and prototype microfluidic devices were fabricated. Proton beam writing with a focused beam is suitable for resolving nanostrucures with high aspect ratios in different resist materials. Using the PPAL system, both large and small structures can be easily combined on the same sample. In the PPAL approach, the pattern writing times are faster than when using the focused beam, however, the resolution is somewhat lower and the patterns can be made up of only rectangular elements. Using improved polishing techniques for the aperture edges and motion drives with a better positioning accuracy can improve the resolution to the sub-100 nm region.

5 Near-edge and surface-scattering

The ultimate resolution performance of the PPAL system is limited by processes taking place at the edges of the aperture. Ion scattering from the aperture edges generates an extra fluence of lower energy ions that are deflected from the original beam incidence direction and may expose the resist in undesirable locations thus deteriorating the resolution performance. Understanding the aperture edge-scattering processes is therefore important which may help to optimise the system performance. Studying the aperture near-edge processes using analytical methods is not straightforward because of the complex geometry of the aperture. Hence, computer simulations using Monte Carlo methods are more appropriate. In this chapter, a study of ion scattering from the aperture in the PPAL geometry using the GEANT4 toolkit is presented. Ion scattering from a cylindrical tungsten carbide roller-bearing used in nuclear microscopy as a beam defining slit is also considered.

5.1 Details of the simulations

The GEANT4 was used to simulate the ion scattering from the aperture edges. The GEANT4 is not a conventional simulation tool (e.g. SRIM [Zieg]), but rather a toolkit written in C++ [Agos03, Alli06]. This toolkit utilises object oriented programming and offers the users a comprehensive set of C++ classes. Using these classes, the users can write their own simulation codes and track desired particles in a user-defined geometry and materials with a required precision. The GEANT4 was originally designed by CERN collaboration for high energy physics applications. The Low Energy Physics package was recently introduced into the toolkit which extended the applicability of the GEANT4 from 1 keV to tens of MeV energy region for ions [G4LowEnergy, GeantPhys]. Constantly being developed and improved, GEANT4 is becoming a standard simulation tool in high energy ion beam based physics. The simulations based on GEANT4 were shown to accurately reproduce experimental results on micrometre scale of ion scattering in thin films [Ince03], making it a useful tool also for studies of ions interaction with the aperture edges.

In our simulations of the ion scattering from the aperture edges, we defined four 100 μm thick metal sheets made of tantalum positioned in space to reproduce the design of the programmable proximity aperture (Fig. 1.1a). A sample, used as an ion detector, was located downstream behind the aperture at a distance L. The detector

recorded the position, energy and the direction of transmitted and edge-scattered ions once they crossed the vacuum-detector boundary. The information was saved in data files which were later processed using numerical analysis software, such as ROOT [Root].

In the preliminary studies on ion scattering from a round edge of a WC cylindrical slit, the slit itself was modelled as a detector that tracked the ions impinging on the slit edge and penetrating though it until they were either stopped (implanted) within the aperture or were ejected. The positions where the ions stopped in the WC slit produced a distribution of implanted hydrogen, while the ejected ions were used to characterise the scattering from the slit edge.

The General Particle Source (GPS) [GenPar] was used to generate the ion beams in the simulations with required lateral and angular distributions of ions.

5.2   Near-edge scattering from a tantalum semi-infinite plate

The ions impinging on the aperture edges may undergo scattering in different scenarios summarised in Fig. 5.1.
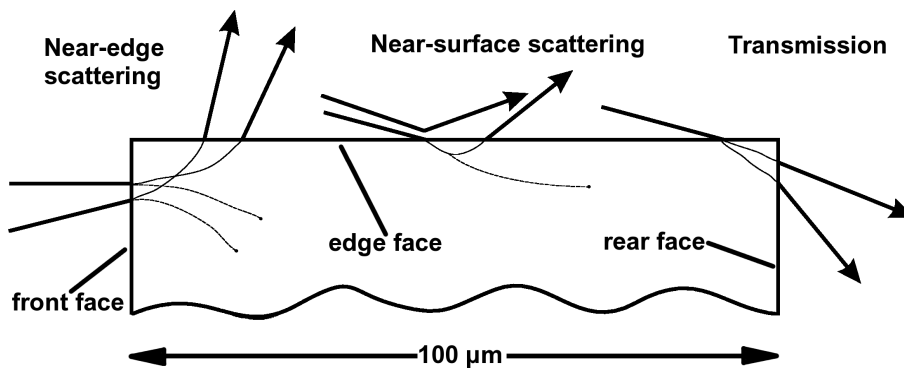

Figure 5.1: Different scenarios of ion scattering from the aperture edge.

For a perfectly parallel beam and the aperture plate aligned precisely with the beam axis, the ions are incident only on the front face of the aperture plate. The fluence of the scattered ions is therefore associated only with the ions that undergo impingement on the front face of the aperture and are scattered in the direction towards the aperture edge-face and are ejected after they crossed the aperture-vacuum boundary. Consequently, the ions that were scattered in the direction opposite to the aperture

edge-face are more likely to be stopped (implanted) in the near-edge region of the aperture.

In real experiments the beams from accelerators are only approximately parallel (or paraxial) with a non-negligible fraction of the beam which is divergent. This leads to an associated impingement of ions on the edge-face of the aperture at glancing[1] angles. Misalignment of the aperture with respect to the beam axis will have similar consequences. The ions impinging on the edge-face of the aperture can be specularly reflected [Wint02], surface-scattered if they penetrate into the aperture [Marw72, Thom78], or ejected (transmitted) if they impinge close to the rear-face of the aperture. Some of the ions can penetrate deep into the aperture and are stopped inside it. In all of these three cases of the near-surface scattering, the ions are deflected away from the original direction of the beam and lose only a fraction of their energy. These deflected ions may broaden the transmitted beam spot and degrade the resolution. The GEANT4 modelling was shown to reproduce the results of the scattering of high energy protons incident at glancing angle on W surface [Kims08]. In the following chapters we investigate the scattering of the ions resulting from the irradiation of the front-face of the apeture plate with a parallel beam of 3 MeV He ions, and the scattering of 3 MeV He ions incident on the Ta aperture edge-face at glancing angles as possible resolution restricting factors.

5.2.1   Parallel beam

In order to characterise the scattering from and transmission through the programmable proximity aperture (PPA) which is made up off four Ta sheets, in the initial study only one 100 μm thick sheet was considered. In a prior study of irradiation of the edge of the Ta sheet with ions originating from a point source and impinging normally on the front face of the aperture at a certain distance d to the edge, we found that only individual He ions were ejected from the edge if the ions impinged at $d >$4 μm. The edge width of the aperture relevant for the edge-scattering was therefore assumed to be equal to 5 μm.

To characterise the ion edge-scattering from a single straight aperture edge, the irradiation of the edge of the Ta sheet positioned at $X > 0$ with a fluence of 3 MeV He ions was simulated (Fig. 5.2a). We chose to concentrate on 3 MeV He ions because this is a primary ion species used in our lithographic applications at the Pelletron accelerator. The angular distribution of the edge-ejected ions is presented in Fig. 5.2b. The distribution, as expected, is symmetric with respect to the Y-axis. The distribution has a maximum at φ=92.56° along the X-axis for the ions scattered to small angles ($<$1°) with respect to the Y-axis. The fluence of the scattered ions on the sample therefore

---

[1] An alternative term for glancing angle, *grazing angle*, is used often in the literature.
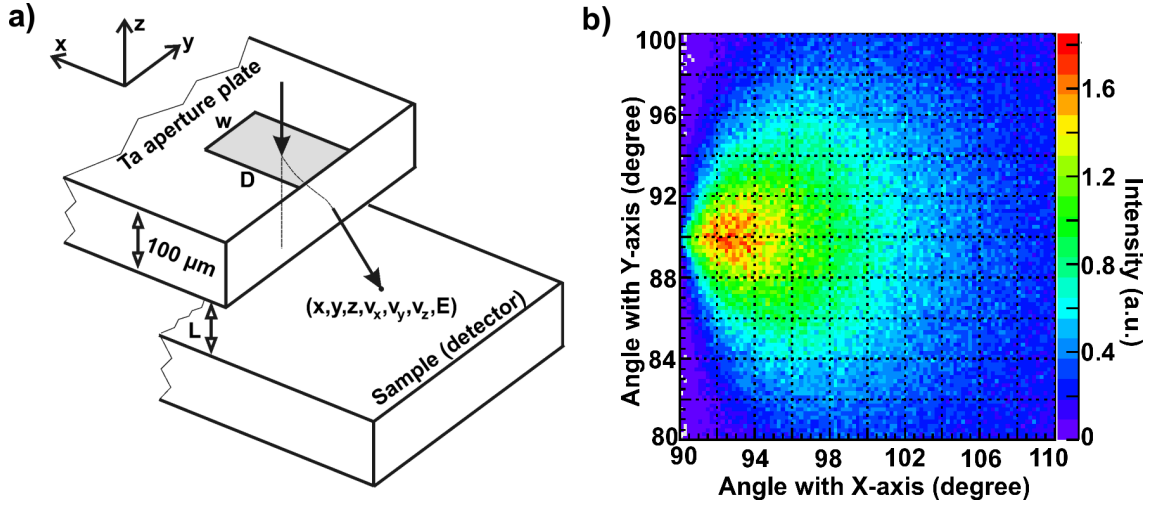
Figure 5.2: a) Edge width $w \times D$ is irradiated with a fluence of ions. The sample positioned at the distance L from the rear face of the aperture plate serves as a sensitive detector that records the entry position into the detector, the direction and the energy of edge-ejected ions. b) Angular distribution of the edge-ejected ions. Note, that because the Ta plate was positioned at $X > 0$, the directions of the edge-ejected ions measured with respect to the X-axis are greater than 90°.

has a maximum intensity at $X_{max} = (t + L)cos(\varphi)$, where t=100 μm is the aperture plate thickness, and L is the distance between the rear face of the aperture plate and the sample (Fig. 5.2a). For instance, for a sample positioned at L=0.5 mm behind the rear face of the aperture plate, the maximum intensity of the fluence of the scattered ions is at X_{max}=600×cos(92.56°)=−26.8 μm from the shadow of the aperture edge[2]. Irradiation of large edge-width w (Fig. 5.2a) of the aperture plate results in an increase of the intensity of the fluence of the scattered ions on the sample. The fluence at the maximum intensity saturates when the value of w is large ($>$80 μm) at a maximum value which depends on the value of L. The calculated maximum fluences at the points of the maximum intensity on the sample are summarised in Fig. 5.3. The fluences at the maximum are two-three orders of magnitude smaller compared to the fluence of the incident beam, therefore the ions scattered from the aperture edge are not likely to cause significant beam spot broadening. However, in applications where well-defined regions of ion-tracks are required, the edge-scattered ions do produce undesirable ion-tracks some ten's of μm outside of the irradiated regions.

---

[2]Since the aperture plate is positioned at $X > 0$, the ions are scattered into the opposite direction, that is into $X < 0$.
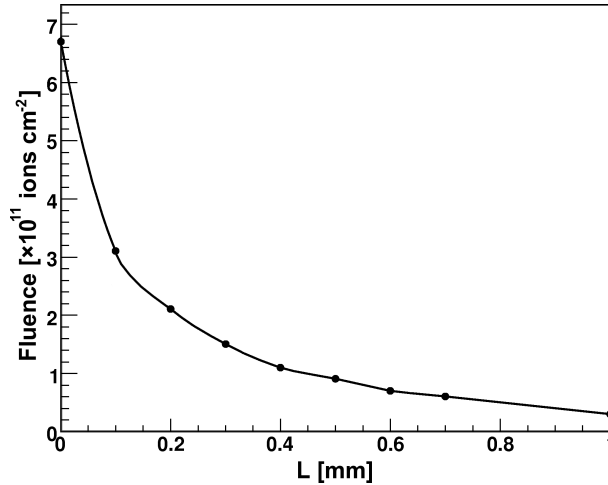
Figure 5.3: Maximum of the fluence of the scattered 3 MeV He ions on the sample resulting from irradiation of a wide edge of the Ta aperture plate plotted as a function of L, the sample-to-aperture separation. The simulated incident fluence of ions is 10^{14} ions cm^{-2}.

5.2.2   Grazing angle of incidence

To characterise the surface-scattering, the irradiation of a width of 1 μm of the Ta aperture plate's edge-face with a fluence of 3 MeV He ions incident on the edge-face at glancing angles (0.2–100 mrad) was simulated with GEANT4. The irradiations were adjusted so that the number of incident ions per unit area of the edge-face was equal to 10^{12} ions cm^{-2} for all incident angles of the beam. The results of such a simulation are presented in Fig. 5.4. The surface-scattered ions are generally deflected to small angles (Fig. 5.4a) and form intense spots on the sample close to the shadow edge of the aperture. The location of the maximum intensity of the fluence of the surface-scattered ions can be found from the maximum of the angular distribution with respect to the X-axis [Paper VI]. Furthermore, the surface-scattered ions undergo only minor energy losses [Paper VI]. By integrating the fluences of the surface-scattered ions resulting from irradiation of the 1 μm width of the edge-face, we find the saturated values of the fluences of surface-scattered ions for different angles of incidence and for different values of L (Fig. 5.4b). The overall fluences of the surface-scattered ions are reduced for smaller angles of incidence (<5 mrad) because smaller Ta edge projected area is exposed to the beam (Fig. 5.5), which is proportional to $t \times \tan(\alpha) \simeq t\alpha$, where t=100 μm is the thickness of the Ta aperture plate. The total fluence of the surface-scattered ions resulting from irradiation of the edge face of the aperture by a beam with 1 mrad divergence with a uniform distribution of the divergent angles within the beam can be found by fitting a polynomial to the plot in Fig. 5.4b and integrating. The calculations indicate that the fluence of the surface-scattered ions is two or less orders of magnitude smaller than the fluence of the incident beam [Paper VI] thus
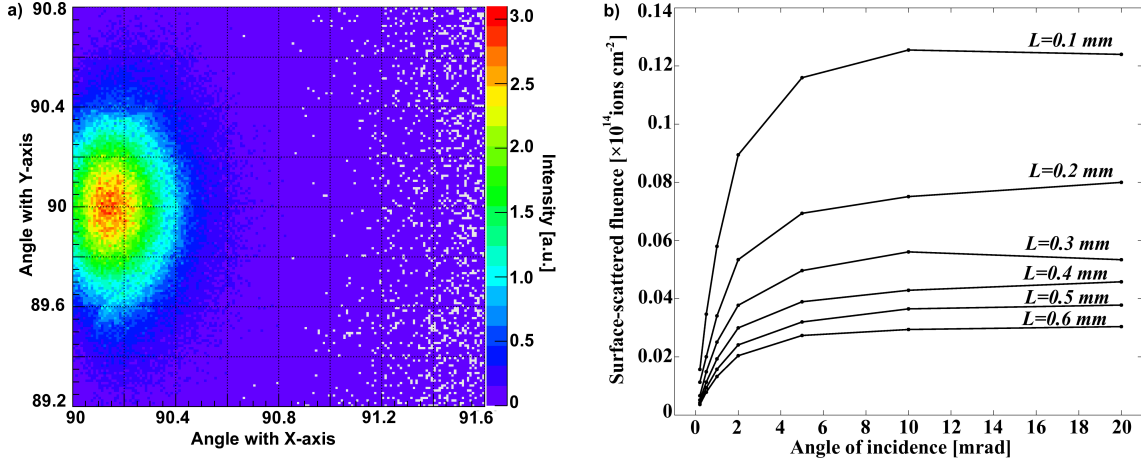
Figure 5.4: Scattering of 3 MeV He ions incident on the edge face of a Ta aperture plate at glancing angles. a) Angular distribution of surface-scattered ions incident on the edge face at 0.5 mrad. b) Maximum of the fluence of the surface-scattered 3 MeV He ions on the sample resulting from irradiation of a large edge-width of the Ta aperture plate plotted as a function of the angle of incidence for different L, the sample-to-aperture separation. The fluences of the surface-scattered ions are normalised to the incident fluence of 10^{14} ions cm^{-2} of the beam through a plane perpendicular to the beam axis.

this extra fluence is also not likely to degrade the beam spot on the sample. However, because the surface-scattered ions lose only a small fraction of their energy and are highly concentrated within just a few μm in the vicinity of the transmitted beam spot, they may have an edge-roughening effect by generating single ion-tracks for a paraxial beam and the aperture plate misalignment with respect to the beam axis. In case of the diverging beam and a good aperture alignment with the beam axis the beam spot broadening effect is primarily caused by the penumbra broadening which is discussed below.

5.3 Scattering from and transmission through an aperture in the PPAL geometry. Penumbra broadening

To investigate the edge-scattering from the Programmable Proximity Aperture (PPA), four 100 μm thick plates made of Ta were defined in space in GEANT4 simulations to form the aperture (Fig. 1.1a). Different aperture openings $a \times b$ were set and the irradiation of the aperture and the aperture edges by a fluence of ions was simulated. Fig. 5.6 shows an example of a simulation for a parallel beam impinging on 1×1 μm aperture opening. The scattered ions create a low intensity (two-three orders of magni-
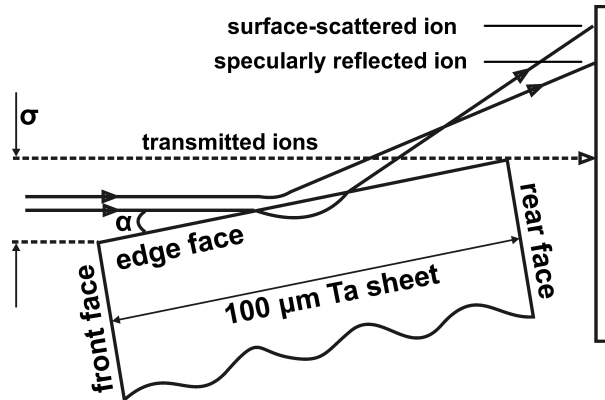
Figure 5.5: For a beam incident on the edge face at a glancing angle α, only a small number of ions from a projected cross-section σ can be surface-scattered from the edge-face of the Ta aperture plate.

tude smaller as compared to the fluence of the incident beam [Paper VII]) asymmetric "halo" spreading to several mm^2 (Fig. 5.6a). The asymmetry of the scattered ions is caused by the asymmetry of the aperture design (Fig. 1.1a). The scattered ions do not deteriorate or broaden the transmitted beam spot which is well-defined and has sharp edges (Fig. 5.6b). In case of divergent beam incidence the fluences of the scattered ions are not considerably different than in the case of a perfectly parallel beam [Paper VII]. The transmitted beam spots are however significantly deteriorated due to the penumbra broadening (Fig. 5.7). The broadening is asymmetric due to the aperture geometry (Fig. 5.8) and is somewhat larger in the Y-direction [Paper VII]. Hence, for exposures with optimal sharpness the structures should have an orientation of the critical pattern dimensions along the X-axis.

5.4   Scattering from a cylindrical aperture edge

Tungsten carbide (WC) roller bearings are commonly used in nuclear microscopy as beam defining slits in object and scraper apertures [Min07, Oxfo]. It has been noted that large low intensity "halos" are present around the focused beam. The intensity of the "halo" typically intensifies after prolonged irradiations. The origin of the "halo" is attributed to the ion scattering from the edge of the beam defining WC slits. Using GEANT4, the angular and energy distributions of edge-scattered protons originating from exposure of the WC cylindrical slit positioned at $X > 0$ and with its axis aligned along the Y-axis with a fluence of 2 MeV protons (Fig.5.9a) were calculated. The angular distribution is, as expected, symmetric with respect to the Y-axis. Most of the protons are scattered to small angles ($<3°$) with about 1% being scattered to $<0.5°$ with respect to the X-axis (Fig. 5.9b). The ejected fraction of the fluence
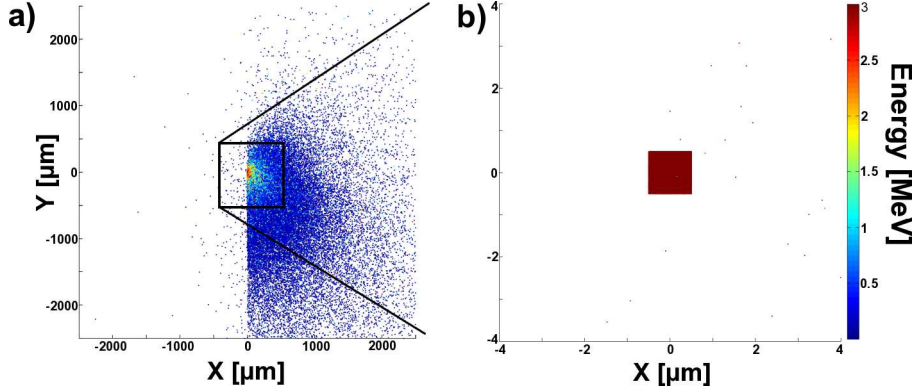
Figure 5.6: a) Spatial distribution and energy of He ions on a sample positioned 0.5 mm behind the PPA resulting from a collimation of a broad perfectly parallel beam of 3 MeV He ions by 1×1 μm aperture opening. b) Zoomed central area from a).

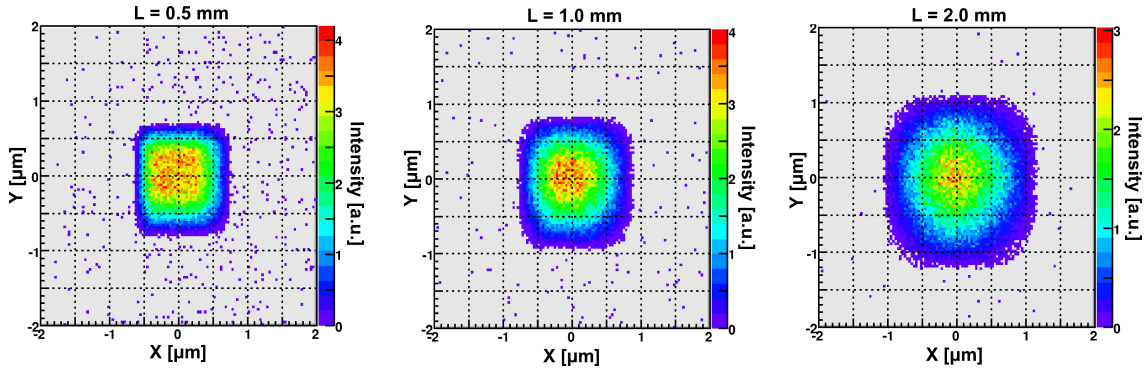**Figure 5.7**: Transmitted beam intensity through 1×1 μm aperture opening on the sample surface for different aperture-sample separations (0.5, 1 and 2 mm). The beam divergence is 0.28 mrad. Uniform distribution of divergent angles within the beam is assumed.

impinging on 1 μm edge projected width is 65% [Paper VIII], with 60% of the ejected protons having the energy loss of less than 300 keV (Fig. 5.9c). Non-negligible fractions of the ejected protons lose only little of their energy. Thus, about 0.36% of the total fluence of the ejected protons lose less than 1 keV; 2.2% lose less than 5 keV; 4.3% lose less than 10 keV. The quadrupole magnetic lenses used to focus the beam are momentum dispersive and hence the ions that have lost only a small amount of their energy, such that they are still transmitted by the lenses, will contribute to the beam spot broadening or to the halo around the beam spot.

The enhancement of the halo after prolonged irradiation might be explained in terms of implanted hydrogen in the tip region of the WC cylinder. Fig. 5.9d shows the calculated distribution of implanted hydrogen in the WC cylinder resulting from irradiation of the slit with a fluence of 10^{14} protons cm^{-2}. The maximum of the implanted concen-
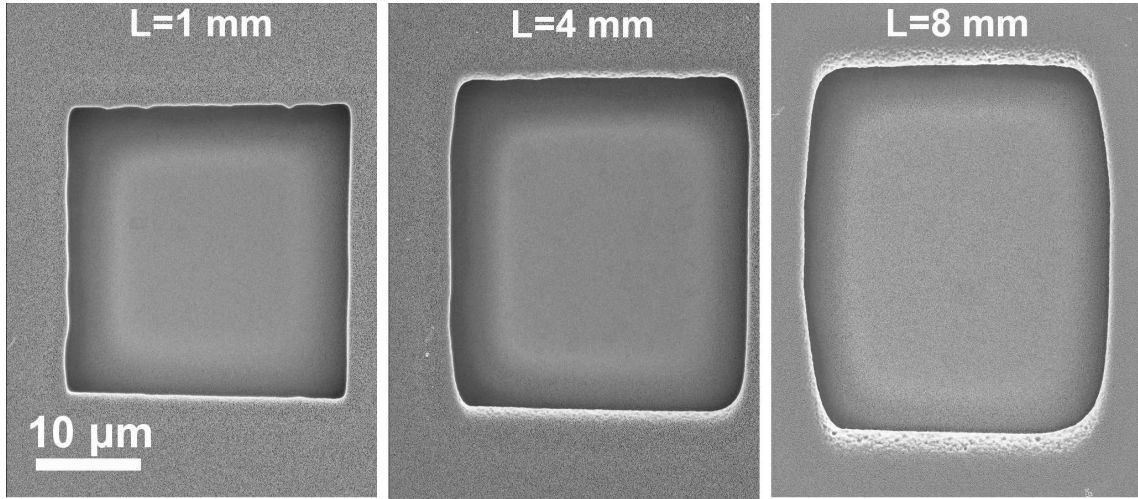
Figure 5.8: Scanning electron microscope images of a rectangular beam spot with a $\sim$25 μm minimum side length written in 7.5 μm PMMA resist using 3 MeV ^{4}He^{2+} ions and developed in a mixture of propan-2-ol and water 7:3 by volume. The sample-aperture distance is varied between 1–8 mm. The beam spot is significantly broadened in the Y-direction.

tration is located upstream of the tip and the concentration is an order of magnitude lower in the tip region. Long irradiations may however lead to large accumulated concentrations of hydrogen at the tip region of the slit. The inclusion of the implanted hydrogen at the tip region of the WC slit will reduce the the density of the material (e.g. through void formation) at the edges. The stopping force exerted on the incident protons will therefore decrease, thus increasing the fraction of the protons that lost only marginal amount of their energy leading to the enhancement of the beam halo on the sample.

5.5   Summary of the chapter

Using GEANT4 various processes at the near-edge region of the apertures can be studied. In this chapter scattering from a straight edge of a Ta aperture plate was investigated in detail. In addition, scattering of ions from the aperture edge face when incident at glancing angles was simulated. The results of the simulations indicate that the aperture edge-scattering is not a resolution restricting factor. The contribution to the beam broadening from the surface-scattered ions incident on the aperture edge face at glancing angles is small but persistent since these ions undergo only minimal energy loss and are scattered into small angles forming a region of enhanced fluence some μm next to the edge of the patterns.
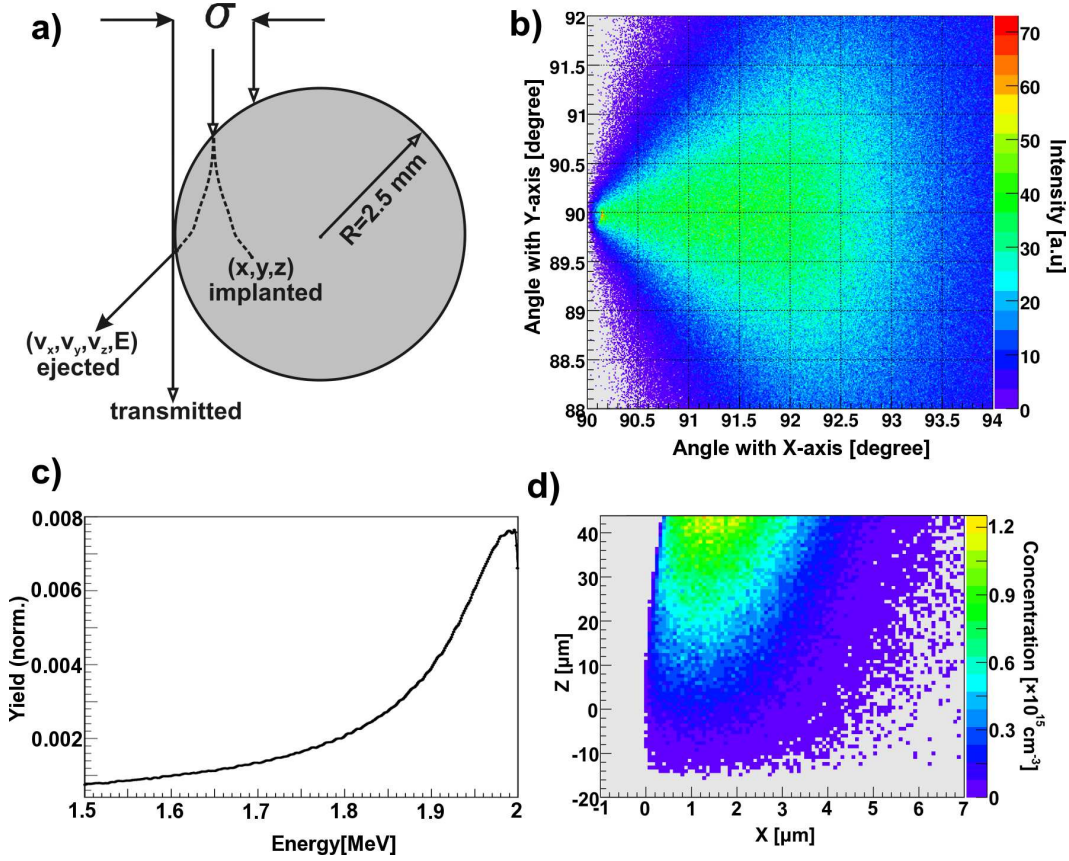
Figure 5.9: Edge effects at the beam defining tungsten carbide (WC) rod. a) A projected width σ of the WC rod which is 5 mm in diameter is irradiated with 2 MeV protons. The WC slit was positioned at $X > 0$ in the simulations. b) Angular distribution of edge-ejected protons that are incident on $\sigma{=}1$ μm. c) Energy distribution of the edge-ejected protons incident on $\sigma{=}1$ μm. d) Distribution of implanted protons in the tip of the WC rod resulting from irradiation with a fluence of 10^{14} protons cm^{-2}. The beam is incident from the $-Z$-direction. The axis of the WC rod is in the Y-direction.

Using GEANT4, ion transmission through complex aperture geometries, such as the PPA, can be investigated. The results of the simulations indicate that the enhancement of the fluence due to the edge-scattering of a parallel beam from the PPA edges is two-three orders of magnitude smaller compared to the incident fluence. The fluence of the edge-scattered ions spreads to several mm^2 and does not cause beam spot degradation. The transmitted beam spots are well-defined and have sharp edges. For diverging beams, the penumbra broadening significantly broadens the beam spot. The broadening is asymmetric due to the asymmetry of the aperture construction. The broadening in the Y-direction is somewhat enhanced relative to that in the X-direction, therefore it is more optimal to design the patterns such that the critical dimensions will be oriented along the X-direction.

In the preliminary investigations of the edge scattering from a cylindrical WC beam defining slit we find that 65% of the fluence of 2 MeV protons incident on the 1 μm edge projected width of the WC slit are ejected. Among the ejected protons, a considerable fraction undergoes only a minimal energy loss. Those protons that lost only a small amount of energy, can be transmitted through the magnetic lenses and impinge on the regions lying outside of the focused beam spot broadening it and generating the halo.

The distribution of implanted hydrogen in the WC slit has a maximum upstream from the tip of the slit. The concentration of the implanted hydrogen at the tip region is reduced, however, long lasting irradiation will lead to accumulation of considerable amount of hydrogen in the tip region. The implanted hydrogen can induce the density decrease of the slit material at the tip region of the WC slit, e.g. through void formation. This will lead to decreased stopping exerted on the incident protons resulting in the increase of the fraction of ejected protons with only a minimal amount of energy loss, hence causing beam spot broadening and enhancement of the beam halo.

6　Conclusion

This thesis deals with development of focused and aperture-based MeV ion beam lithographies and their applications for bioengineering and microfluidics. Using MeV ions for lithography applications offers a number of advantages when compared with more conventional lithographies utilizing electron beams and UV or X-ray radiation. Among these advantages is the possibility to fabricate high aspect ratio structures with straight walls in thick resist films in a direct write process. Such structures have a potential application in biomedical research where the information on cellular response to three dimensional surface geometry is required for the success of tissue engineering.

Using proton beam writing, test cell-growth substrates were fabricated and growth of osteoblasts on these substrates was studied. The results of this preliminary study indicate that the cellular behaviour on different surfaces is remarkably different, and different surface geometries can potentially be used to control the cellular behaviour and proliferation.

Proton beam writing is very suitable for production of high aspect ratio nanostructures in a variety of resist materials. In a study of nickel electroplating using hydrogen silsequioxane (HSQ) structures as molds, we found that the adhesion of individual high aspect ratio HSQ nanostructures to Ti/Si substrates is excellent. The adhesion to Cr/Si is comparable to Ti/Si, however, because of the debris formation around the HSQ nanostructures presumably induced by the proton irradiation, the Cr/Si substrates are not optimal.

The direct write methods benefit from simplicity and flexibility but suffer from low production speed. The novel lithography method that combines the advantages of the direct write method and the mask exposure, Programmable Proximity Aperture Lithography (PPAL), has been developed in Jyväskylä. In this method the samples are exposed through a rectangular variable-size computer-controlled aperture, which allows rapid exposures of complex patterns. The experimental and theoretical results presented in this thesis indicate that this method is very suitable for fabrication of microstructures with the smallest structures realized until now well into the deep sub-μm region. The resolution performance of the PPAL system is primarily governed by the beam divergence, the aperture edge quality and the motional precision of the positioners that set the dimensions of the aperture opening. The resolution of the PPAL system thus can be further refined by introducing improved polishing methods of the

aperture edges and installing more precise motion drives. It is therefore evident that the PPAL system has a great future promise and could be used for nanofabrication. Significantly, such a system does not require a major investment into the equipment and can be installed at nearly any accelerator, both large, such as a cyclotron, and small, such as an electrostatic Pelletron accelerator. In this thesis, the PPAL system has been tested at two accelerators with satisfactory performance.

The ion-aperture edge interactions play a key role in MeV ion beam lithography when defining the beam size both in shadow casting (such as in PPAL) and when writing with a focused beam (e.g. PBW). The ion scattering from the aperture edges could broaden the beam size and degrade the resolution. In this thesis, the ion-aperture edge interactions were studied using the GEANT4 toolkit. The calculations indicate that the ion scattering from the straight aperture edges in the PPAL is not a resolution restricting factor but instead the resolution is primarily limited by the beam divergence. In the focused ion beam lithography, the scattering from a cylindrical edge of the tungsten carbide beam defining slit is substantial. These results are important for understanding the limitations of the MeV ion beam system which ultimately rely on the beam collimation. Knowing these limitations, new designs of apertures or collimators with reduced edge scattering can be developed.

Appendix A: PMMA sample preparation

All the sample preparation was conducted in a clean room environment. Typical substrates for microstructure fabrication were rectangular Si pieces cut from Si wafers. The Si substrates are cleaned in hot acetone followed by a rinse in propan-2-ol (IPA) and blow dried in flowing N_2. For biomedical applications transparent substrates are required. In this case rectangular pieces are cut from glass cover slips. The glass substrates were cleaned in chromic acid solution for about 10 min, followed by an intensive washing in deionized water and rinse in either in IPA or in ethanol. The glass substrates were then baked at 180 °C immediately prior to the resist deposition to dehydrate the surface.

PMMA resist was spin-coated at 2500 rpm from a PMMA A11 solution (11% PMMA in anisole). The solution was purchased from MicroChem [MicroChem]. Spinning is followed by a soft-bake at 180 °C for 5 min which evaporates the solvent and yields a 2.5 μm thick PMMA layer. Repeating the spinning yields thicker films, e.g. three spinnings result in 7.5 μm thick PMMA layer.

After the exposures the PMMA samples are developed in IPA:deionized water (7:3 by volume) solution for 4–6 min, followed by a double rinse in deionized water and N_2 blow-drying.

Appendix B: HSQ sample preparation

All the sample preparation was carried out in a clean room environment. Typical substrates for microstructure fabrication were rectangular Si pieces cut from Si wafers. The Si substrates are cleaned in hot acetone followed by a rinse in propan-2-ol (IPA) and blow-dried in flowing N_2.

When necessary, the substrates were coated with thin metal films of Au, Cr and Ti by electron beam evaporation, Ar sputtering and Filtered Cathodic Vacuum Arc (FCVA) deposition.

The substrates were baked at 150 °C immediately prior to the resist deposition to dehydrate the surface.

HSQ resist was spin-coated at 3000 rpm from a FOX-17 solution. The solution was purchased from Dow Corning [DowC]. Spinning is followed by a soft-bake at 150 °C for 2 min which evaporates the solvent and yields a 1.2 μm thick HSQ layer.

After the exposures the HSQ samples are developed in 2.38% tetramethyl ammonium hydroxide (TMAH) solution for 60 sec, followed by rinsing in deionized water. The samples are then either dried under N_2 flow or left drying under the clean room fumehood's airflow.

Appendix C: PPAL patterns

The pattern is specified in a simple ASCII file arranged as sequential blocks of six records. The first line is a rectangular keyword, *!RREC*, is used to separate different pattern elements. The second and third lines are the coordinates $(X1, Y1)$ in μm of the upper left corner of the rectangular to be exposed. The fourth and fifth lines are the coordinates $(X2, Y2)$ μm of the lower right corner of the rectangular. The sixth line is the exposure time in seconds. The structure of the PPAL file together with the visualized pattern is shown in Fig. 1. The pattern files can be loaded into the purpose-built LabView software, *LiSy* – Lithography System, that performs automated exposures. For compatibility, the LiSy software also accepts the CIBA group .emc file formats [Bett05].
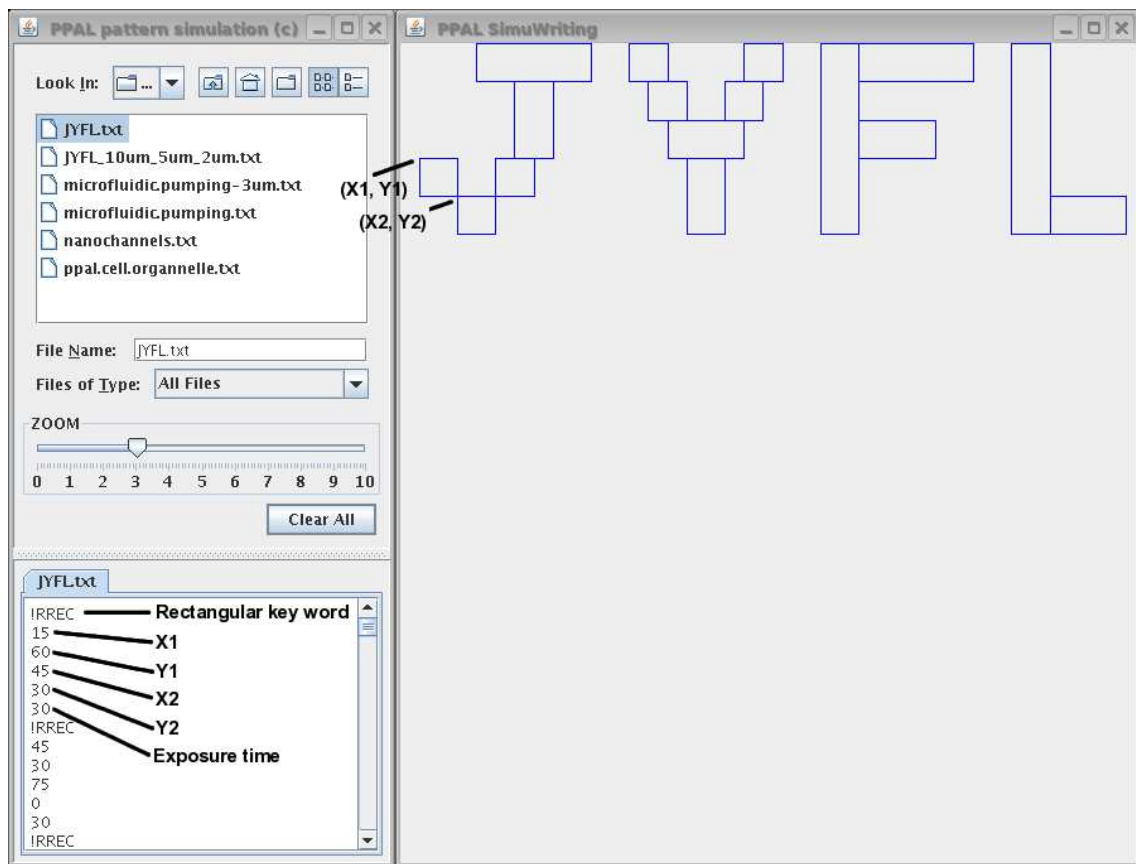

Figure 1: The patterns for the PPAL system are specified in ASCII files. The specilized JAVA-software can be used to preview the patterns.

Some of the most relevant functions implemented in the LiSy-software package are as follows:

- Moving both the aperture and sample stages.

- Built-in "anti-collision" control that prevents erroneous movement of the stages that would otherwise result in the collision of the aperture Al blocks (Fig. 3.2a) or in an out-of-the-range position.

- Setting the aperture opening.

- Beam blanking.

- Fully automated exposures.

- (optional) Beam current measurement and setting of the aperture calibration [Paper IV].

Appendix D: Other publications by the author not included in this thesis

1. <u>S. Gorelick</u>, Z. Fang, J.A. van Kan, H.J. Whitlow, F. Watt, *Ni electroplating of proton beam micromachined HSQ resist,* submitted to Nucl. Inst. Meth. B (2008).

2. S. Sangyuenyongpipat, S. Ikonen, V. Marjomäki, T. Sajavaara, A. Sagari A.R., <u>S. Gorelick</u>, M. Laitinen, L. Wang, H.J. Whitlow, *Development of micro-contact printing of osteosarcoma cells using MeV ion beam lithography,* submitted to Nucl. Inst. Meth. B (2008).

3. M. Laitinen, I. Riihimäki, J. Ekman, A.R. Ananda Sagari, L.B. Karlsson, S. Sangyuenyongpipat, <u>S. Gorelick</u>, H. Keittunen, H. Penttilä, R. Hellborg, T. Sajavaara, H.J. Whitlow, *Mobility determination of lead isotopes in glass for retrospective Radon measurements,* Radiation Protection Dosimetry (2008) doi:10.1093/rpd/ncn162.

4. A. Sagari A.R., P. Rahkila, M. Väisänen, R. Lehto, T. Sajavaara, <u>S. Gorelick</u>, M. Laitinen, M. Putkonen, S. Sangyuenyongpipat, J. Timonen, S. Cheng, H.J. Whitlow, *Wettability and compositional analysis of hydroxyapatite films modified by low and high energy ion irradiation,* Nucl. Inst. Meth. B 266 (2008) 77.

5. A. Sagari A.R., C. Lautaret, <u>S. Gorelick</u>, P. Rahkila, M. Putkonen, K. Arstila, T. Sajavaara, S. Cheng, H.J. Whitlow. *Ion-sputtering deposition of Ca-P-O films for microscopic imaging of osteoblast cells,* Nucl. Inst. Meth. B 261 (2007) 719.

6. <u>S. Gorelick</u>, T. Sajavaara, M. Laitinen, N. Puttaraksa, H.J. Whitlow, *Resolution Performance of Programmable Proximity Aperture MeV Ion Beam Lithography System,* Mater. Res. Soc. Symp. Proc. 1020 (2007) 67.

References

[Paper I] S. Gorelick, P. Rahkila, A. Sagari A.R., T. Sajavaara, S. Cheng, L.B. Karlsson J.A. van Kan, H.J. Whitlow, Nucl. Inst. Meth. B 260 (2007) 130.

[Paper II] S. Gorelick, F. Zhang, J.A. van Kan, H.J. Whitlow, F. Watt, *Adhesion of proton beam written high aspect ratio Hydrogen Silsesquioxane (HSQ) nanostructures on different metallic substrates*, J. Vac. Sci. Technol. B (2009) submitted.

[Paper III] S. Gorelick, T. Ylimäki, T. Sajavaara, M. Laitinen, A. Sagari A.R., H.J. Whitlow, Nucl. Inst. Meth. B 260 (2007) 77.

[Paper IV] N. Puttaraksa, S. Gorelick, T. Sajavaara, M. Laitinen, S. Singkarat, H.J. Whitlow, *Programmable proximity aperture lithography with MeV ion beams*, J. Vac. Sci. Technol. B (2008) accepted.

[Paper V] S. Gorelick, N. Puttaraksa, T. Sajavaara, M. Laitinen, S. Singkarat, H.J. Whitlow, Nucl. Inst. Meth. B 266 (2008) 2461.

[Paper VI] S. Gorelick, T. Sajavaara, H.J. Whitlow, *Aperture edge scattering in MeV ion beam lithography. Part I: scattering from a straight Ta aperture edge*, J. Vac. Sci. Technol. B. (2009) submitted.

[Paper VII] S. Gorelick, T. Sajavaara, H.J. Whitlow, *Aperture edge scattering in MeV ion beam lithography. Part II: scattering from a rectangular aperture*, J. Vac. Sci. Technol. B. (2009) submitted.

[Paper VIII] S. Gorelick, H.J. Whitlow, *Aperture edge scattering in focused MeV ion beam lithography and nuclear microscopy: an application for the GEANT4 toolkit*, Nucl. Inst. Meth. B. (2009) submitted.

[Agos03] S. Agostinelli et. al., Nucl. Instr. and Meth. A 506 (2003) 250. GEANT4 available from http://www.geant4.org/geant4/

[Alli06] J. Allison et. al., IEEE Transactions on Nuclear Science 53 (2006) 270.

[Amse03] G. Amsel, G. Battistig, A. L'Hoir, Nucl. Inst. Meth. B 201 (2003) 325.

[Baek05] I.-B. Baek, J.-H. Yang, W.-J. Cho, C.-G. Ahn, K. Im, S. Lee, J. Vac. Sci. Technol. B 23 (2005) 3120.

[Bett02] A.A. Bettiol, I. Rajta, E.J. Teo, J.A. van Kan, F. Watt, Nucl. Instr. and Meth. B 190 (2002) 154.

[Bett05] A.A. Bettiol, C.N.B. Udalagama, J.A. van Kan, F. Watt, Nucl. Instr. Meth. B 231 (2005) 400.

[Cham03] C.N.B Udalagama, A.A Bettiol, J.A. van Kan, F. Watt, Nucl. Instr. and Meth. B 210 (2003) 256.

[Cham07] C.N.B. Udalagama, A.A. Bettiol, F. Watt, Nucl. Instr. and Meth. B 260 (2007) 384.

[Delf2000] F.C.M.J.M. van Delft, J.P. Weterings, A.K. van Langen-Suurling, H. Romijn, J. Vac. Sci. Technol. B 18 (2000) 3419.

[Delf02] F.C.M.J.M. van Delft, J. Vac. Sci. Technol. B 20 (2002) 2932.

[DowC] FOX-17® FLOWABLE OXIDE. Data sheet is available from http://www.dowcorning.com

[G4LowEnergy] Design and source code available from http://www.ge.infn.it/geant4/lowE/index.html

[GeantPhys] GEANT4 Physics Reference, available from http://geant4.web.cern.ch/geant4/UserDocumentation/UsersGuides/ PhysicsReferenceManual/fo/PhysicsReferenceManual.pdf

[GenPar] General Particle Source package, available from http://reat.space.qinetiq.com/gps/

[Gore09d] S. Gorelick, Z. Fang, J.A. van Kan, H.J. Whitlow, F. Watt, *Ni electroplating of proton beam micromachined HSQ resist*, Nucl. Inst. Meth. B. (2009) submitted.

[Helb05] R. Hellborg, *Electrostatic Accelerators Fundamentals and Applications*, ISBN: 978-3-540-23983-3, Springer-Verlag Berlin Heidelberg (2005).

[Ince03] S. Incerti, Ph. Barberet, B. Courtois, C. Michelet-Habchi, Ph. Moretto, Nucl. Inst. Meth. B 210 (2003) 92.

[JYFL] Information on Jyväskylä K130 cyclotron is available at http://www.jyu.fi/science/laitokset/fysiikka/en/research/accelerator/accelerator/k130/

[Kims08] P. Kimsrand, N. Tilly, A. Ahnesjö, E. Traneus, Phys. Med. Biol. 53 (2008) 1115.

[Laba98] J.G.C. Labanda, S.A. Barnett, L. Hultman, J. Vac. Sci. Technol. B 16 (1998) 1885.

[Lewi50] H.W. lewis, Phys. Rev. 78 (1950) 526.

[Liuk92] E. Liukkonen, in: Proceedings on the 13th International Conference on Cyclotrons and their Applications, Vancouver, 1992, p. 22

[Mado02] M.J. Madou, *Fundamentals of microfabrication: the science of miniaturization* 2nd ed., ISBN: 0-8493-0826-7 (2002).

[Marw72] A.D. Marwick, M.W. Thompson, B.W. Farmery, G.S. Harbinson, Radiation Effects 15 (1972) 195.

[Marw75] A.D. Marwick, P. Sigmund, Nucl. Inst. Meth. 126 (1975) 317.

[MicroChem] Nano^{TM} PMMA and copolymer data sheet, MicroChem Corp., http://www.microchem.com
PMMA data sheet is available from
http://www.microchem.com/products/pdf/PMMA_Data_Sheet.pdf

[Min07] R. Min-Qin, *Nuclear microscopy: Development and applications in atherosclerosis, Parkinson's disease and materials physics*, PhD thesis, Research report No. 6/2007, University of Jyväskylä.

[Nama98] H. Namatsu, Y. Takahashi, K. Yamazaki, T. Yamaguchi, M. Nagase, K. Kurihara, J. Vac. Sci. Technol. B 16, 69 (1998).

[Oxfo] OM10 Precision differential micrometre controlled beam defining slits, Oxford Microbeams Ltd., http://microbeams.co.uk

[Rahk] P. Rahkila, private communication.

[Root] ROOT - an object-oriented data analysis framework, available from http://root.cern.ch

[Saga07] A.R.A. Sagari, C. Lautaret, S. Gorelick, M. Laitinen, P. Rahkila, M. Putkonen, K. Arstila, T. Sajavaara, S. Cheng, H.J. Whitlow, Nucl. Instr. and Meth. B 261 (2007) 719.

[Scot63] W. Scott, Rev. Mod. Phys. 35 (1963) 231.

[Sigm74] P. Sigmund, K.B. Winterbon, Nucl. Inst. Meth. 119 (1974) 541.

[Sigm78] P. Sigmund, J. Heinemeier, F. Besenbacher, P. Hvelplund, H. Knudsen, Nucl. Inst. Meth. 150 (1978) 221.

[Tayl06] M.L. Taylor, R.D. Franich, A. Alves, P. Reichart, D.N. Jamieson, P.N. Johnston, Nucl. Instr. and Meth. B 249 (2006) 752.

[Tayl07] M.L. Taylor, A. Alves, P. Reichart. R.D. Reichart. S. Rubanov, P. Johnston, D.N. Jamieson, Nucl. Instr. and Meth. B 260 (2007) 426.

[Tiro07] R. Tiron, L. Mollard, O. Louveau, E. Lajoinie, J. Vac. Sci. Technol. B 25 (2007) 1147.

[Thom78] M.W. Thompson, H.J. Pabst, Radiation Effects 37 (1978) 105.

[vanE06] J. van Erps, B. Volckaerts, H. van Amerongen, P. Vynck, R. Krajewski, C. Debaes, J. Watte, A. Hermanne, H. Thienpont, IEEE Photonics Technology Letters 18 (2006) 1164.

[vanK99] J.A. van Kan, J.L. Sanchez, B. Xu, T. Osipowicz, F. Watt, Nucl. Inst. Meth. B 158 (1999) 179.

[vanK03] J.A. van Kan, A.A. Bettiol, F. Watt, Mat. Res. Soc. Symp. Proc. Vol. 777 (2003) T2.1.1.

[vanK04] J.A. van Kan, A.A. Bettiol, K. Ansari, E.J. Teo, T.C. Sum, F. Watt, International Journal of Nanotechnology 4 (2004) 464.

[vanK05] J.A. van Kan, P.G. Shao, P. Molter, M. Saumer, A.A. Bettiol, T. Osipowitz, F. Watt, Nucl. Inst. Meth. B 231 (2005) 170.

[vanK06] J.A. van Kan, A.A. Bettiol, F. Watt, Nano Letters 6 (2006) 579.

[vanK07] J.A. van Kan, A.A. Bettiol, F. Watt, Nucl. Instr. and Meth. B 260 (2007) 398.

[vanK07a] J.A. van Kan, P.G. Shao, K. Ansari, A.A. Bettiol, T. Osipowicz, F. Watt, Microsystem Technologies 13 (2007) 431.

[Volc2000] B. Volckaerts, H. Ottevaere, A. Vila, M. Muruzabal, C. Debaes, P. Vynck, P. Tuteleers, V. Baukens, A. Hermanne, I. Veretennicoff, H. Thienpont, Optical MEMS, 2000 IEEE/LEOS International Conference, Kauai, HI, USA (2000) 103.

[Wahb06] T. Wahbrink, D. Küpper, Y.M. Georgiev, J. Bolten, M. Möller, D. Küpper, M.C. Lemme, H. Kurz, Microelectron. Eng. 83 (2006) 1124.

[Wali86] M.P.R. Waligorski, R.N. Hamm, R. Katz, Nucl. Tracks Radiat. Meas 11 (1986) 309.

[Watt05] F. Watt, A.A. Bettiol, J.A. van Kan, E.J. Teo, M.B.H. Breese, International Journal of Nanoscience 4 (2005) 269.

[Watt97] F. Watt, Nucl. Instr. and Meth. B 130 (1997) 1.

[Watt07] F. Watt, M.B.H. Breese, A.A. Bettiol, J.A. van Kan, Materials Today 10 (2007) 20.

[Weiss97] M. Weißing, M. Batzill, K.J. Snowdon, Nanotechnology 8 (1997) 40.

[Whit04] H.J. Whitlow, M.L. Ng, V. Auzelyte, I. Maximov, L. Montelius, J.A. van Kan, A.A. Bettiol, F. Watt, Nanotechnology 15 (2004) 223.

[Wint02] H. Winter, Physics Reports 367 (2002) 387.

[Word03] M.J. Word. I. Adesida, P.R. Berger, J. Vac. Sci. Technol. B 21 (2003) L12.

[Yama07] I. Yamada, Nucl. Instr. Meth. B 257 (2007) 632.

[Yasi02] S. Yasin, D.G. Hasko, H. Ahmed, Microelectron. Eng. 61–62 (2002) 745.

[Zieg] J.F. Ziegler, J.P. Biersack, SRIM - The Stopping and Range of Ions in Matter, available from http://srim.org